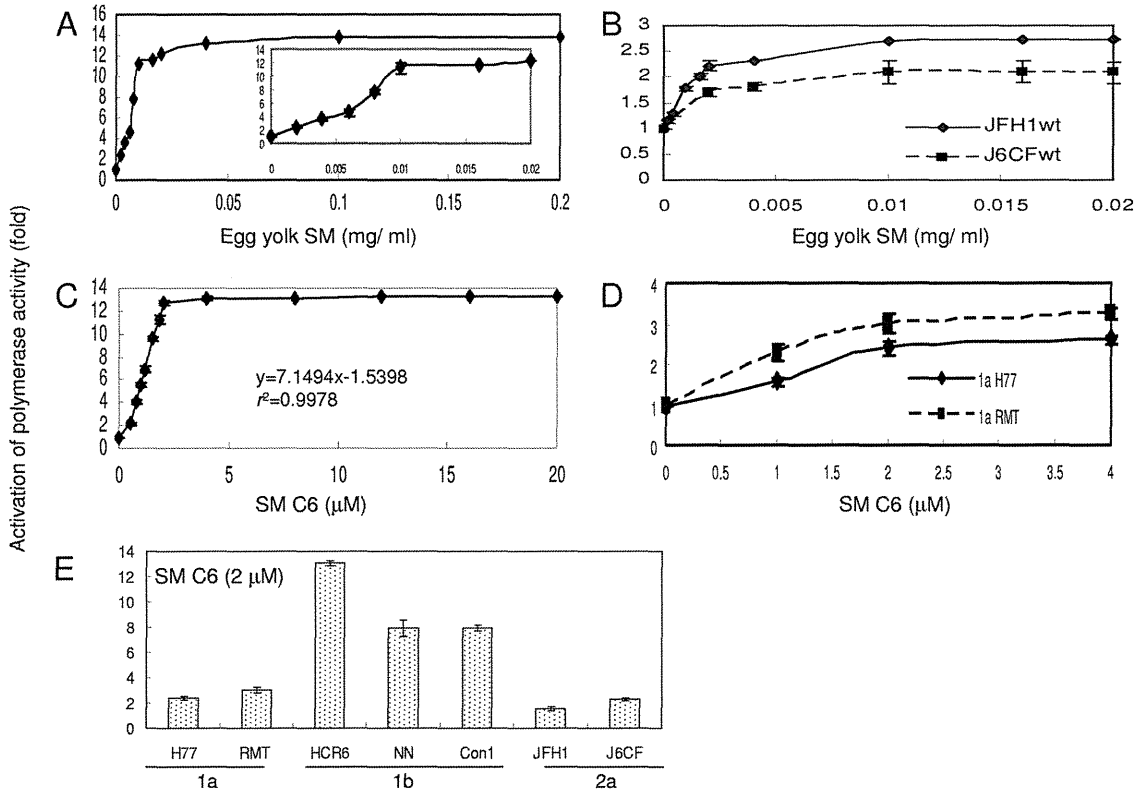

FIG. 1. Sphingomyelin activation of HCV RNA polymerases. (A) Activation kinetics of HCV HCR6 (1b) RdRp wt by egg yolk sphingomyelin (SM). The inset shows activation produced by 0 to 0.02 mg/ml egg yolk sphingomyelin. Activation kinetics of HCV 2a (JFH1 and J6CF) RdRps by egg yolk sphingomyelin (B) and of HCV HCR6 (1b) RdRp wt by hexanoyl sphingomyelin (SM C6) (C). In panel C, the first order of the graph was fitted by linear regression; the calculated equation is indicated in the graph. (D) Activation kinetics of HCV 1a (H77 and RMT) RdRps by hexanoyl sphingomyelin. (E) Activation effect of hexanoyl sphingomyelin on HCV RdRp of various genotypes. HCV RdRp (100 nM) was incubated with or without 2 μM SM C6. The names of the RdRps are indicated below the graph. Mean ± standard deviation of the activation ratio was calculated from three independent experiments.

RdRp wt, its activation kinetics were calculated using hexanoyl sphingomyelin (Fig. 1C, SM C6). The equation for the first-order ratio of hexanoyl sphingomyelin activation according to linear regression fitting was as follows: $y = 7.1494x - 1.5398$, where y is the activation ratio and x is the sphingomyelin concentration ($r^2 = 0.9978$). RdRp activation had almost plateaued at 2 μM hexanoyl sphingomyelin. The activation kinetics of JFH1 (2a) and J6CF (2a) RdRps in egg yolk sphingomyelin were biphasic and plateaued at 0.01 mg/ml. Those of RMT (1a) and H77 (1a) RdRps in hexanoyl sphingomyelin were also biphasic and plateaued at 2 μM. The curve of the first order was fitted by linear regression. The molar ratio of RdRp to hexanoyl sphingomyelin at its plateau was calculated as 1:20.

Because RdRp activation had almost plateaued at 2 μM hexanoyl sphingomyelin, we compared the effect of sphingomyelin on 100 M concentrations of RNA polymerases of the HCV 1a, 1b, and 2a genotypes using 2 μM hexanoyl sphingomyelin (Fig. 1E and Table 1).

Helix-turn-helix structure for sphingomyelin binding and activation. Sphingomyelin binds to the SBD peptide (see HCV SBD in Fig. 7) (29). Initially, we tested whether SBD was the sphingomyelin binding site in HCV RdRp by ELISA (Fig. 2A and Table 1). When the L245 and I253 residues of the SBD peptide were mutated to A, sphingomyelin binding activity was lost (29). We introduced the same mutations in HCV HCR6 (1b) RdRp and purified HCR6 (1b) RdRp with mutations L245A, I253A, and L245A/I253A. Because the C-terminal His-tagged HCR6 RdRp(L245A/I253A) was not soluble, it was solubilized by tagging of glutathione *S*-transferase (GST) sequence at the N terminus but lost polymerase activity. As the L245A/I253A mutant had lost its polymerase activity, polymerase activation was tested only for L245A and I253A (Fig. 2B and Table 1). These results confirmed that SBD located in the finger domain (residues 230E to 263G) successfully achieved sphingomyelin binding in HCV RdRp and that sphingomyelin did not bind to the SBD when the helix-turn-helix structure had been destroyed by the L245A or I253A mutation (29).

The sphingomyelin binding activities of genotype 1a and 2a RdRps were also tested (Fig. 2 and Table 1). Both JFH1 and J6CF were tested for genotype 2a because J6CF (2a) RdRp had an additional amino acid difference at position 241 in the SBD, and its sphingomyelin binding activity was very low (Fig. 2A and 7A; Table 1). J6CF (2a) RdRp(R241Q) showed the same sphingomyelin binding activity as HCR6 (1b) RdRp wt, indicating that 241Q was the critical amino acid for sphingomyelin binding. J6CF (2a) RdRp(S244D) and RdRp(R241Q/S244D) also showed higher sphingomyelin binding activity

TABLE 1. Summary of sphingomyelin activation of HCV RNA polymerase activities

Parameter	Value for the parameter by RdRp genotype, strain, and variant[a]																							
	1b							1a							2a									
	HCR6					NN	Con1	RMT	H77		J6CF				JFH1									
	wt	L245A	I253A	L245A/I253A	D244S	wt	wt	wt	wt	A238S/Q248E	wt	R241Q	S244D	R241Q/S244D	wt	A242C	S244D	A242C/S244D	T251Q
SM binding (%)[b]	100	24.3	30.8	15.5	78.7	93.4	117	144	86.7	82.5	19.3	118	53.1	80.2	70.4	75.5	93.1	92.4	80.7
Activation of polymerase (*n*-fold)[c]	13.0 (11.2)[d]	(2.8)[d]	(2.5)[d]	ND	3.6	7.9	7.9	3.0	2.0	8.1	2.3	4.3	5.6	3.4	1.6	1.0	3.1	4.4	1.8
Activation of RNA binding (*n*-fold)[c]	4.5	2.6	1.7	ND	1.9	ND	ND	ND	1.4	3.3	1.5	3.6	3.2	1.7	1.3	ND	ND	1.4	ND

[a] Numbers were averaged from three independent experiments. ND, not done.
[b] Egg yolk sphingomyelin (SM; 250 ng) was used.
[c] Hexanoyl sphingomyelin (2 μM) was used.
[d] Egg yolk sphingomyelin (0.01 mg/ml) was used.

than the wt ($P < 0.001$) but lower binding than the R241Q mutant. However, S244D showed higher RdRp activation than R241Q ($P < 0.005$), while the RdRp activation ratio of the double mutant (R241Q/S244D) was lower than that of S244D or R241Q, although all of them activated RdRp with sphingomyelin ($P < 0.005$) (Fig. 2A and C and Table 1). For JFH1, when the JFH1 RdRp SBD was modified (A242C/S244D) to allow it to bind with more sphingomyelin than the wt ($P < 0.005$), the mutant JFH1 RdRp(A242C/S244D) was activated more than the wt by sphingomyelin ($P < 0.005$) (Fig. 2A and C; Table 1). The sphingomyelin binding activity of JFH1 RdRp(T251Q) was 80.7% of that of HCR6 (1b), and its activation ratio was 1.8-fold. These results agree that SBD is both the sphingomyelin activation and binding domain and that the domains for these two activities are somehow different.

We determined which amino acid, 242C or 244D, enhanced sphingomyelin binding by comparing HCR6 (1b) and JFH1 (2a) RdRps. Sphingomyelin binding of HCR6 (1b) RdRp(D244S) was 79% of that of the wt ($P < 0.005$) (Fig. 2A and Table 1), and its activation by sphingomyelin was only 3.6-fold (Fig. 2C and Table 1). The sphingomyelin binding of JFH1 (2a) RdRp(A242C) and RdRp(S244D) increased to 75.5% and 93.1%, respectively, of HCR6 (1b) RdRp wt (Fig. 2A and Table 1). This was significantly higher than that of JFH1 (2a) RdRp wt ($P < 0.005$), and the sphingomyelin activation of JFH1 (2a) RdRp(A242C) and RdRp(S244D) was increased 1.0-fold and 3.1-fold, respectively ($P < 0.005$) (Fig. 2C and Table 1). From these mutation analyses of the J6CF and JFH1 RdRps, we concluded that 244D enhanced sphingomyelin binding and RdRp activation.

HCV 1a RdRps were not activated even though sphingomyelin bound to them (Fig. 1E and 2A and Table 1). We then tried to elucidate the domains responsible for sphingomyelin activation. There are 14 amino acids (residues 19, 25, 81, 111, 120, 131, 184, 270, 272, 329, 436, 464, 487, and 540) unique to genotype 1a RdRp in the region of residues 1 to 570 and two amino acid differences unique to 1a RdRp in SBD, i.e., 238A and 248Q (see Fig. 6A). Initially, we focused on the SBD and introduced the A238S and Q248E mutations into the H77 (2a) RdRp SBD (Fig. 2A and D and Table 1). The sphingomyelin binding activity of H77 (2a) RdRp(A238S/Q248E) was similar to that of H77 (2a) RdRp wt. The sphingomyelin activation ratio of H77 (2a) RdRp(A238S/Q248E) was increased 8.1-fold, leading us to conclude that these mutations are essential to sphingomyelin activation.

Effect of lipids on HCV RNA polymerase activity. In order to elucidate the structure of the lipids involved in activation of HCV RdRp, D-lactosyl-β-1,1′-*N*-octanoyl-D-*erythro*-sphingosine [C_8-lactosyl(β) ceramide], D-glucosyl-β1-17-N-octanoyl-D-*erythro*-sphingosine (C_8-β-D-glucosyl ceramide), *N*-hexanol-D-*erythro*-sphingosine (C_6-ceramide), and cholesterol were tested for their abilities to activate RdRp. The relative polymerase activities of 100 nM HCV HCR6 (1b) RdRp activated with 0.01 mg/ml egg yolk sphingomyelin, 2 μM hexanoyl sphingomyelin, 8 μM C_8-lactosyl(β) ceramide, 12 μM C_8-β-D-glucosyl ceramide, 12 μM C_6-ceramide, and 0.02 mg/ml cholesterol were 11.2, 13.0, 5.66, 4.19, 1.12, and 2.25 of that without lipids, respectively (Fig. 3A). The amount of lipids that gave the maximum activation was calculated from the kinetics of the lipids bound to HCR6 (1b) and JFH1 (2a) RdRps (Fig. 3B and

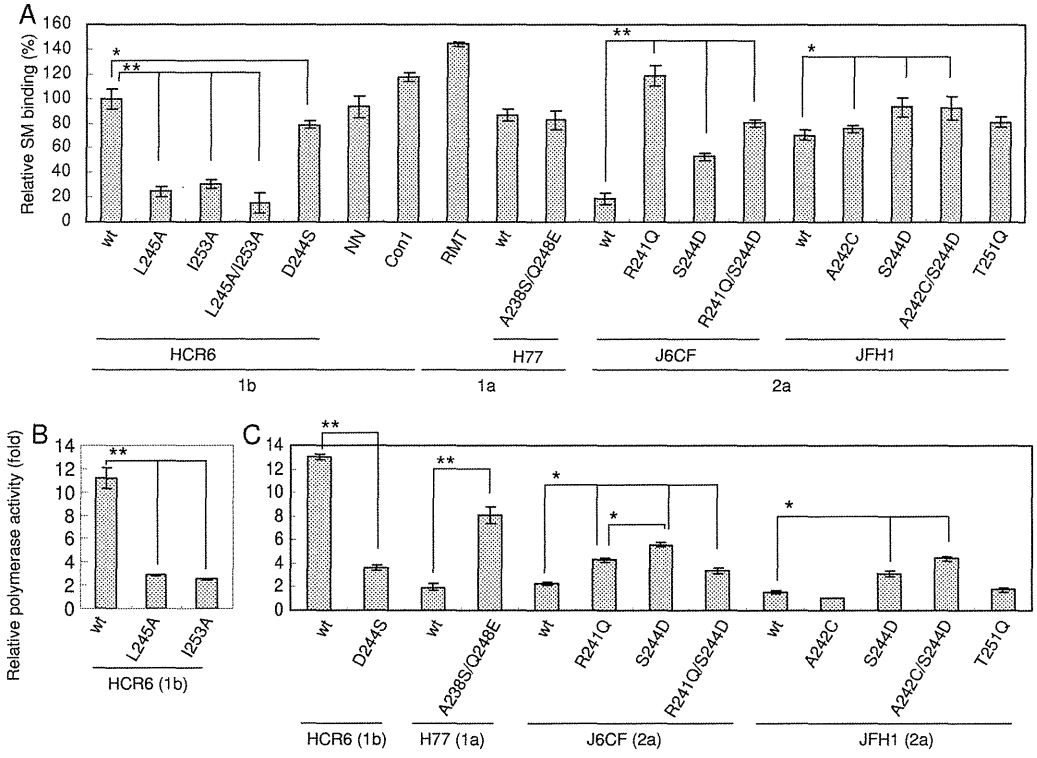

FIG. 2. Sphingomyelin binding and activation of HCV RNA polymerase sphingomyelin binding domain mutants. Names of RdRps are indicated below the graphs. (A) Egg yolk sphingomyelin (SM) binding activity relative to that of HCR6 (1b) RdRp wt. Mean ± standard deviation of the binding was calculated from three independent experiments. (B) Egg yolk sphingomyelin activation of HCR6 (1b) RdRps. RdRps (100 nM) were incubated with or without 0.01 mg/ml egg yolk sphingomyelin. (C) Hexanoyl sphingomyelin activation of the RdRps (RdRp names are indicated below the graphs). HCV RdRps (100 nM) were incubated with or without 2 μM hexanoyl sphingomyelin. The mean ± standard deviation of the activation ratio was calculated from three independent experiments. *, $P < 0.005$; ** $P < 0.001$.

C). C_8-lactosyl(β) ceramide and C_8-β-D-glucosyl ceramide activated HCR6 (1b) RdRp compared with the linear regression kinetics of the reaction with hexanoyl sphingomyelin as it plateaued (Fig. 1C and 3B). Cholesterol activated HCR6 (1b) RdRp slightly but did not activate JFH1 (2a) RdRp (Fig. 3C). We therefore concluded that the phosphocholine of sphingomyelin bound to the SBD of HCV RdRp because the order of HCV RdRp activation was hexanoyl sphingomyelin > C_8-lactosyl(β) ceramide > C_8-β-D-glucosyl ceramide, and C_6-ceramide did not activate HCV HCR6 (1b) RdRp. The polarity of the phosphocholine of sphingomyelin is important for HCV RdRp activation (see Fig. S5 in the supplemental material).

In order to test whether phosphocholine activated HCV RdRp (Fig. 3D), HCR6 (1b) RdRp was incubated with 0.4, 2, 20, 100, and 400 μg and 2, 4, 11, 54, and 100 mg of phosphocholine. Up to 400 μg of phosphocholine did not affect RdRp activity, but more than 2 mg of phosphocholine inhibited RdRp activity.

Effect of sphingomyelin on the template RNA binding of HCV RNA polymerase. The mechanism of HCV RdRp activation was analyzed. RNA polymerase changes its conformation throughout the different transcription steps, and template binding is the first step of transcription (9). Therefore, the effect of sphingomyelin on template RNA binding activity was tested (Fig. 4A and Table 1). Sphingomyelin enhanced the template RNA binding of HCR6 (1b) RdRp wt but not that of JFH1 (2a), H6CF (2a), or H77 (1a) wt RdRp. When the A238S/Q248E mutation was introduced into H77 (1a) RdRp, the RNA binding was enhanced. J6CF (2a) RdRp R241Q and S244D mutants showed similar enhancement of RNA binding, but the R241Q/S244D double mutant did not. The activation effect of RNA binding of HCR6 (1b) RdRp mutants L245A, I253A, and D244S was lower than that of RdRp wt. JFH1 (2a) RdRp wt and RdRp(A242C/S244D) showed similar RNA binding activation levels. Based on a comparison of the sphingomyelin activation of HCR6 (1b) RdRp wt and its mutants which lost sphingomyelin binding with J6CF (2a) RdRp wt and the R241Q and S244D mutants and H77 (1a) RdRp wt and the A238S/Q248E mutant, we concluded that polymerase activation by sphingomyelin was induced mainly via activation of the template RNA binding of RdRp. RNA binding activity of JFH1 (2a) RdRp wt and RdRp(A242C/S244D) was almost saturated because RNA binding of these RdRps was not activated by sphingomyelin (see Fig. S4 in the supplemental material).

HCV RdRp has to be bound with sphingomyelin before or at the same time as it binds to template RNA. After RdRp had bound to the template RNA, sphingomyelin did not enhance template RNA binding strongly (Fig. 4B).

Effect of the sphingomyelin binding domain mutations for HCV replicon activity with myriocin. In order to confirm sphingomyelin activation of HCV polymerase activity in a viral replication system, HCV replicon activity of the loss-of-function mutant HCV NN (1b) NS5B(D244S) and the gain-of-

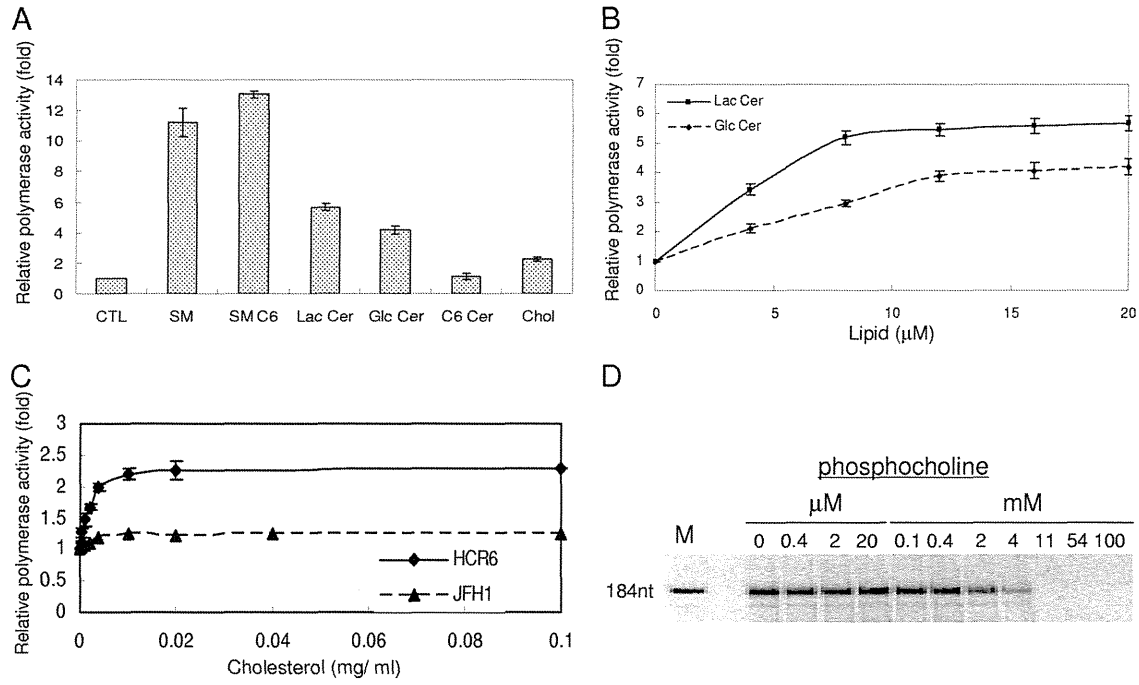

FIG. 3. HCV RNA polymerase activation effect of lipids. (A) Lipid activation of HCR6 (1b) RdRp wt. HCV HCR6 (1b) RdRp wt (100 nM) was incubated with or without (control [CTL]) 0.01 mg/ml egg yolk sphingomyelin (SM), 2 μM hexanoyl sphingomyelin (SM C6), 8 μM C_8-lactosyl(β) ceramide (Lac Cer), 12 μM C_8-β-D-glucosyl ceramide (Glc Cer), 12 μM C_6-ceramide (C6 Cer), or 0.02 mg/ml cholesterol (chol). (B) Activation kinetics of C_8-lactosyl(β) ceramide (Lac Cer) and C_8-β-D-glucosyl ceramide (Glc Cer) on HCR6 (1) RdRp. (C) Activation kinetics of cholesterol on HCR6 (1b) and JFH1 (12a) RdRps. (D) The effect of phosphocholine on HCR6 (1b) RdRp. The mean ± standard deviation of the activation ratio was calculated from three independent experiments.

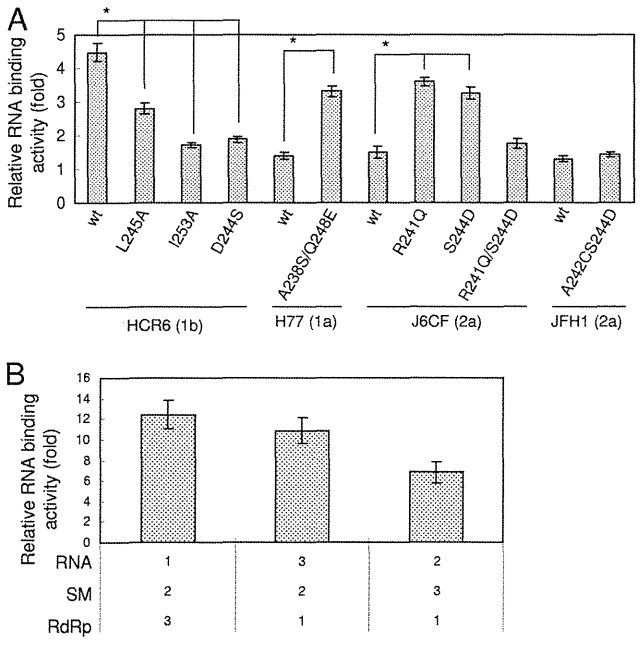

FIG. 4. Sphingomyelin activation of the RNA binding activity of HCV RNA polymerase. (A) Sphingomyelin activation of RNA filter binding of HCV RdRps (RdRp names are indicated below the graph). RdRps and ^{32}P-labeled RNA template (SL12-1S) were incubated with or without egg yolk sphingomyelin (SM), before filtration. (B) Effect of the order of sphingomyelin treatment. Numbers below the graph indicate the order in which the reagents were added. The graph represents the ratio to RNA binding without sphingomyelin. The mean ± standard deviation of the activation ratio was calculated from three independent experiments. *, $P < 0.01$.

function mutants H77 (1a) NS5B(A238S/Q248E) and JFH1 (2a) NS5B(A242C/S244D) were compared with 5 and 50 nM myriocin treatment for 72 h (Fig. 5).

First, HCV replicon activity was compared as the relative luciferase activity (Fig. 5A). Both JFH1 (2a) wt and NS5B(A242C/S244D) replicons showed similar and strong replicon activity ($133 \times 10^3 \pm 12 \times 10^3$ and $138 \times 10^3 \pm 8.5 \times 10^3$, respectively). JFH1 (2a) wt replicon was resistant to myriocin treatment, as reported by Aizaki et al. using other SPT inhibitors (3). The JFH1 (2a) NS5B(A242C/S244D) replicon became sensitive to myriocin but still showed higher replicon activity than NN (1b) or H77 (1a) replicons even at 50 nM myriocin.

To analyze the effect of mutations precisely, the replicon activity relative to each wt strain was compared (Fig. 5B). The JFH1 (2a) wt replicon with 50 nM myriocin showed the same luciferase activity as the wt without myriocin (102% ± 9.6%). JFH1 (2a) NS5B(A242C/S244D) replicon activity was the same as that of the wt without myriocin (103% ± 12%); with 5 nM myriocin it was 84.1% ± 6.6% of the wt level, but with 50 nM myriocin it was 70.3% ± 5.3% of the wt level, which was significantly lower ($P < 0.01$). NN (1b) wt replicon activity was 45.3% ± 6.6% with 5 nM myriocin and 21.7% ± 2.9% with 50 nM myriocin relative to the wt level without myriocin. NN (1b) NS5B(D244S) replicon activity was 72.2% ± 12% without myriocin ($P < 0.05$), 44.0% ± 7.4% with 5 nM myriocin, and 38.1% ± 4.2% with 50 nM myriocin relative to wt level without myriocin, which was significantly higher ($P < 0.01$). Thus, NN (1b) NS5B(D244S) showed lower replicon activity than the wt

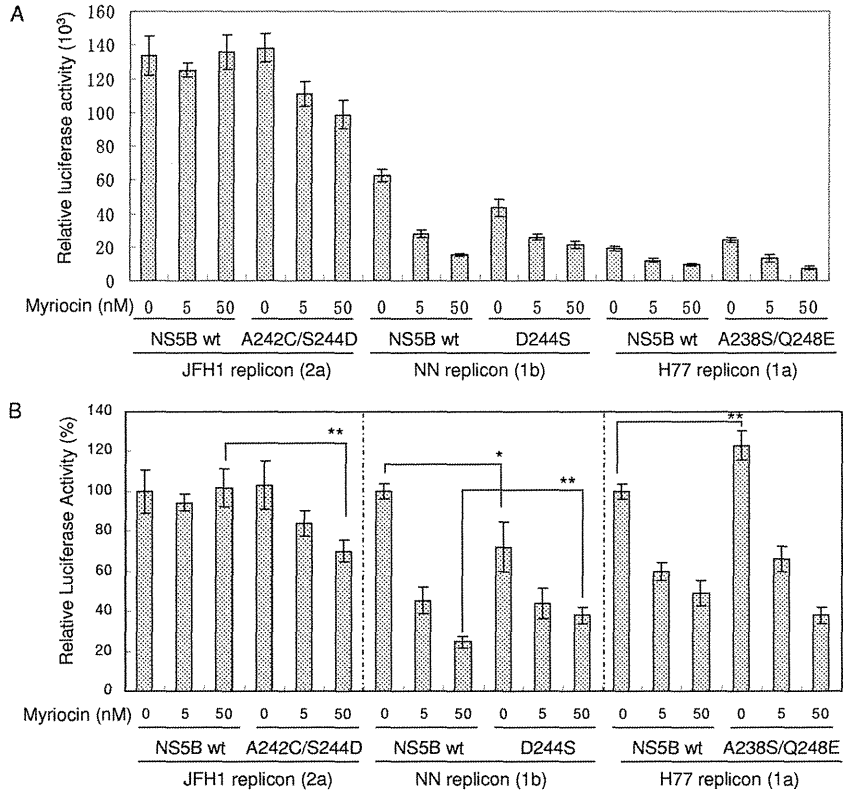

FIG. 5. Myriocin inhibition of HCV replicon activity. Huh7.5.1 cells were incubated with myriocin after transfection with the HCV replicons indicated below the graphs. Means ± standard deviations of the relative luciferase activity at 72 h after myriocin treatment compared to activity at 4 h after transfection (A) and to that of each wt without myriocin (B) were calculated from three independent measurements. *, $P < 0.05$; ** $P < 0.01$.

and was less sensitive to myriocin than the wt. H77 (1a) wt replicon activity was 59.9% ± 4.2% with 5 nM myriocin and 49.2% ± 6.4% with 50 nM myriocin relative to the wt level without myriocin. H77 (1a) NS5B(A238S/Q248E) replicon activity was 123% ± 7.1% without myriocin ($P < 0.01$), 66.1% ± 6.3% with 5 nM myriocin, and 38.0% ± 4.1% with 50 nM myriocin relative to wt level without myriocin. Both H77 (1a) wt and NS5B(A238S/Q248E) replicons were sensitive to myriocin, and the replicon activity of NS5B(A238S/Q248E) was higher than that of the wt.

JFH1 (2a) RdRp(A242C/S244D) localized in the DRM fractions. Myriocin sensitivity of JFH1 (2a) NS5B(A242C/S244D) replicon indicates the importance of 244D in JFH1 NS5B for sphingomyelin binding. To further confirm the role of 244D for recruitment of HCV RdRp to the detergent-resistant membrane (DRM), where the HCV replication complex exists, we compared the distribution of NS5A and NS5B of JFH1 (2a) wt and NS5B(A242C/S244D) in their replicon cells by sucrose density gradient centrifugation of the DRM (Fig. 6). NS5A proteins of both JFH1 (2a) wt and NS5B(A242C/S244D) replicons localized in the DRM fraction where caveolin-2 was present (11, 27), but most of NS5B wt localized in the Triton-soluble fractions. NS5B of JFH1 (2a) NS5B(A242C/S244D) replicon was shifted to the DRM fraction from the soluble fraction. The shift of NS5B(A242C/S244D) localization into the DRM demonstrated that SBD was the DRM localization domain of NS5B and that residue 244D was important for this localization.

DISCUSSION

Hepatitis C virus is an envelope virus, and the lipid components of the virion play important roles in HCV infectivity and virion assembly (3, 15, 20, 24). HCV replication complexes localize in lipid raft structures/DRMs in the membrane frac-

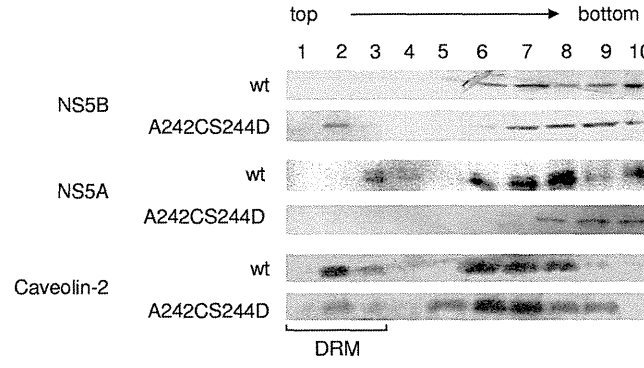

FIG. 6. Membrane floating assay of JFH1 wt and NS5B(A242C/S244D) replicon cells. The PNS fractions of HCV JFH1 (2a) wt and NS5B(A242C/S244D) replicon cells were treated with 1% Triton X-100 in TNE buffer for 30 min at 4°C and subjected to 10 to 40% sucrose gradient centrifugation in TNE buffer. Each fraction was subjected to 10% SDS-PAGE, followed by Western blotting with anti-NS5A, -NS5B, and -caveolin-2 antibodies. Fractions are numbered as indicated at the top of the panel. The DRM fractions (fractions 1 to 3) are indicated.

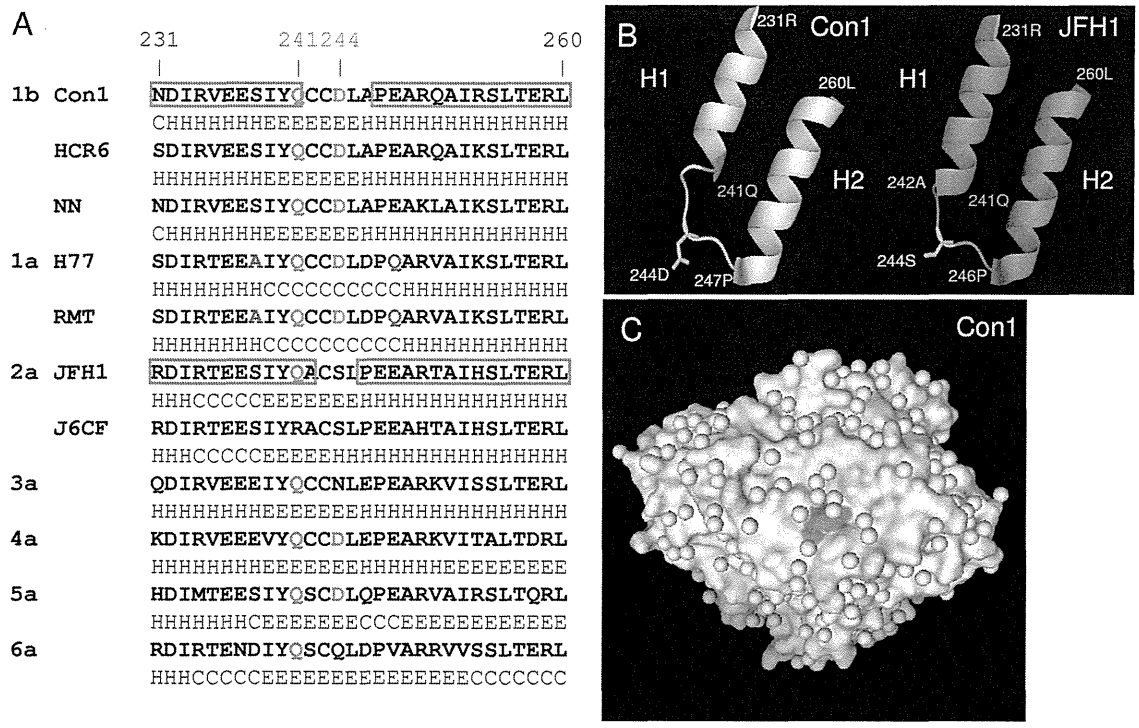

FIG. 7. Sphingomyelin binding domain (SBD) of HCV RNA polymerase. (A) The SBDs (231N to 260L) of HCV RdRps are aligned together with their secondary structure predicted by the Chou-Fasman program (10). The predicted secondary structure is indicated below the sequence as follows: H, α-helix; E, β-sheet; and C, coil. The α-helix structures of HCV Con1 (1b) RdRp and JFH1 (2a) RdRp are boxed in red. Residues 241Q and 244D are indicated in red and green, respectively. The 238A and 248E of the H77 and RMT (1a) RdRps are indicated in purple. GenBank accession numbers of HCV genotypes 3a, 4a, 5a, and 6a are GU814263 (12), GU814265 (12), Y13184 (8), and Y12083 (1), respectively. (B) Comparison of the SBDs of HCV Con1 (1b) (yellow) and JFH1 (2a) RdRps (magenta). The starting and ending amino acids of H1 and H2 are indicated. The sphingomyelin binding site, 241Q, is indicated in red, and 244D of Con1 (1b) and 244S of JFH1 (2a) RdRp are indicated in green. (C) Surface model of HCV Con1 (1b) RdRp. SBD is indicated in yellow, and 241Q and 244D are indicated in red and green, respectively. The structures of the Con1 and JFH1 RdRps were constructed by PyMOL, version 1.1.1 (http://www.pymol.org/). PDB numbers of Con1 (1b) RdRp and JFH1 (2a) RdRp are 3FQL (14) and 3I5K (31), respectively.

tions of subgenomic replicon cells (30). Lipid rafts are composed mainly of sphingomyelin, cholesterol, and glycosphingolipids. Most reports regarding the relationship between lipids and HCV have examined virion assembly, infectivity, and the localization of HCV, but their biochemical interactions have not been reported. Our findings clearly demonstrate that sphingomyelin plays an important role not only in HCV replication complex formation and its localization but also in HCV RdRp activity.

The helix-turn-helix structure of the SBD (residues 230 to 263), which is located between RNA polymerase motifs A and B, has been proposed as the sphingomyelin binding domain of HCV RdRp (29). We compared the SBD of Con1 (1b) (Protein Data Bank [PDB] 3FQL) (14) and JFH1 (2a) (PDB 3I5K) (31) and the secondary structure of the amino acids (201 to 290) in the SBD predicted by the Chou-Fasman program (10) (Fig. 7; see also Fig. S5 in the supplemental material) because the helix structures of the SBD of Con1 (helix 1 [H1], 231N to 241Q; helix 2 [H2], 247A to 260L) and JFH1 (H1, 231R to 242A; H2, 246P to 260L) RdRp fit with those predicted by the Chou-Fasman program. The structures contributing to sphingomyelin binding and activation are H1 and H2 and the junction (turn) between the two helix structures that are similar to the human immunodeficiency virus (HIV) gp120 V3 domain, prion protein (PrP), and β-amyloid peptide (13, 22). Although Con1 (1b) RdRp has a shorter helix structure than JFH1 (2a) RdRp (Fig. 6B), the structures of their SBDs are very similar (Fig. 7; see also Fig. S5). When the helix-turn-helix structure of the SBD was destroyed (HCR6 genotype 1b RdRp mutants L245A and I253A), the RdRp lost sphingomyelin binding activity and lost its activation (Fig. 2).

In order to study the structure-function relationship of the SBD and sphingomyelin, we compared the SBD of genotype 1a, 1b and 2a RdRps and particularly focused on residue 244D in the turn and residues 241Q and 238S/248E in the helix domains. The polar amino acid 241Q and the negatively charged 244D of Con1 (1b) RdRp located on the surface of the RdRp molecule bind and interact with the positively charged choline residue of sphingomyelin (Fig. 7C; see also Fig. S5 in the supplemental material). The positively charged 241R repels the choline residue of sphingomyelin, and as a result, J6CF (a) RdRp wt did not bind to sphingomyelin. J6CF (2a) RdRp(R241Q) showed almost the same sphingomyelin binding activity as HCR6 (1b) RdRp wt. This ionic interaction between SBD and sphingomyelin agrees with the activation of lipids with different sphingosine structures and fatty acid chains (Fig. 3A). JFH1 (2a) RdRp does not interact well with sphingomyelin because it does not have the negatively charged

amino acids at the tip of its turn structure. Once its 244S was changed to D, more sphingomyelin bound to JFH1 (2a) RdRp and activated the RdRp (Fig. 2A and C). The reason for the low activation of J6CF (2a) RdRp(R241Q/S244D) is not clear. Sometimes mutations affect the entire conformation of the molecule. In conclusion, from the comparison of sphingomyelin binding and activation of HCR6 (1b), J6CF (2a), and JFH1 (2a) RdRp SBD mutants, 241Q is the essential amino acid for sphingomyelin binding in the SBD. Amino acid 244D enhanced both binding and RdRp activation.

The *in vitro* sphingomyelin binding and RdRp activation experiments indicate that sphingomyelin binding and its RdRp activation are different biochemical reactions because we found controversial activation rates for sphingomyelin binding and RdRp activation among J6CF (2a) RdRp mutants (Fig. 2). The relationship between sphingomyelin binding and the activation of polymerase activity was studied by comparing genotype 1b and 1a RdRps, both of which bind to sphingomyelin (Fig. 2). However, 1a RdRp is not activated by sphingomyelin because both of the helix structures of 1a RdRp are probably terminated at 238A and 248Q, making its helix structures shorter than those of 1b RdRp (Fig. 6A). The length of the helix structure may be essential for sphingomyelin activation because RdRp changes its structure to bind to template RNA when sphingomyelin binds to SBD (Fig. 4).

HCV RdRp changes its conformations at the early stages of transcription initiation, including the template RNA binding step (6, 9). Sphingomyelin binding is likely to change the conformation of 1b RdRp to recruit template RNA and initiate transcription efficiently. Comparison of the activation ratio of RNA binding and polymerase activity of 1b RdRp, J6CF (2a) RdRp wt and R241Q and S244D mutants, and JFH1 (2a) RdRp wt and mutant A242C/S244D suggests that steps other than RNA binding are also likely to be activated by sphingomyelin.

From a kinetic analysis of sphingomyelin activation (Fig. 1C and D), 20 sphingomyelin molecules are estimated to interact with the SBD of RdRp and activate it because sphingomyelin activation plateaued at 20 sphingomyelin molecules per HCV RdRp molecule. It is not clear whether 20 sphingomyelin molecules form a micelle or a layer structure. However, the structure of sphingomyelin is important for the activation of HCV RdRp because phosphocholine did not activate the RdRp (Fig. 3D).

To confirm these biochemical findings in HCV replication, we tested the effect of SBD mutations in HCV replicon systems with the SPT inhibitor myriocin (Fig. 5) (4, 33) because NA255 was not available. The loss-of-function mutant, HCV NN (1b) NS5B(D244S), showed lower replicon activity than NN (1b) wt and more resistance to 50 nM myriocin, which did not affect the viability of cells (4, 33), than the wt. The gain-of-function mutant, H77 (1a) NS5B(A238S/Q248E), showed higher replicon activity than H77 wt and retained myriocin sensitivity because it had the sphingomyelin binding sites 241Q and 244D. At 50 nM myriocin, another gain-of-function mutant, JFH1 (2a) NS5B(A242C/S244D), was inhibited although its activity was the same as that of JFH1 (2a) wt without myriocin because the JFH1 wt replicon had high replicon activity without myriocin (Fig. 5A). The JFH1 replicon activity may be maximal in the system; therefore, the JFH1 (2a) NS5B(A242C/S244D) replicon did not show higher activity than JFH1 (2a) wt without myriocin while H77 (1a) NS5B(A238S/Q248E) showed higher replicon activity than H77 wt.

The binding and RdRp activation activity of the amino acid 244 mutants by sphingomyelin did not differ greatly from the wt *in vitro*. However, the myriocin sensitivity of JFH1 (2a) NS5B(S244D) was demonstrated clearly. That of H77 (1a) NS5B(A238S/Q248E) indicated that sphingomyelin binding was the target of myriocin inhibition, not the sphingomyelin activation of RdRp. These data confirm the importance of 241Q, 244D, and the helix structure in SBD for HCV replication in the cells.

Sphingomyelin is the major component of the lipid raft structure/DRM where the HCV genome replicates. To confirm that the SBD is the membrane binding site of HCV RdRp, we analyzed the localization of NS5B of JFH1 (2a) wt and NS5B(A242C/S244D) replicons by membrane floating assay (Fig. 6). JFH1 (2a) NS5B wt did not localize in the DRM. However, the localization of NS5B of the JFH1 (2a) NS5B(A242C/S244D) replicon shifted to the DRM from the soluble fractions. Previously, HCV NS5B was believed to localize in the DRM by its C-terminal hydrophobic sequences (21). However, our data demonstrate that the SBD is the membrane localization domain of HCV NS5B, which agrees with the myriocin sensitivity of JFH1 (2a) NS5B(A242C/S244D) replicons (Fig. 5) and the release of HCV 1b NS5B from the DRM by another SPT inhibitor, NA255 (29).

This is the first report of RNA polymerase activation by lipids. Twenty sphingomyelin molecules interact with SBD, particularly with residues 241Q and 244D of HCV (1b) RdRp, and change the conformation of the RdRp in order to recruit RNA templates. At the same time, HCV RdRp molecules may be aligned on the sphingomyelin layer formed via interactions between the hydrocarbon chains of sphingosine and fatty acids via placement of their SBD into the layer (Fig. 7C). Consistent with previous research (3, 23, 37), our findings explain why the inhibitors of the sphingolipid biosynthetic pathway influence subgenomic replicons derived from HCV genotypes 1a and 1b but not those derived from JFH1 (2a) (Fig. 5). Most HCV isolates have 241Q in NS5B, and some of them also have 244D (Fig. 7A). These sphingomyelin interactions are new targets for the treatment of HCV.

ACKNOWLEDGMENTS

We thank C. Rice and R. Bartenshlager for the HCV H77 and Con1 plasmids, respectively. We also thank F. Chisari for Huh7.5.1 and Huh7/src cells.

This work was supported by a grant-in-aid from the Chinese Academy of Sciences (O514P51131 and KSCX1-YW-10), the Chinese 973 project (2009CB522504), and the Chinese National Science and Technology Major Project (2008ZX10002-014).

REFERENCES

1. **Adams, N. J., R. W. Chamberlain, L. A. Taylor, F. Davidson, C. K. Lin, R. M. Elliott, and P. Simmonds.** 1997. Complete coding sequence of hepatitis C virus genotype 6a. Biochem. Biophys. Res. Commun. **234:**393–396.
2. **Aizaki, H., K. J. Lee, V. M. Sung, H. Ishiko, and M. M. Lai.** 2004. Characterization of the hepatitis C virus RNA replication complex associated with lipid rafts. Virology **324:**450–461.
3. **Aizaki, H., K. Morikawa, M. Fukasawa, H. Hara, Y. Inoue, H. Tani, K. Saito, M. Nishijima, K. Hanada, Y. Matsuura, M. M. Lai, T. Miyamura, T. Wakita, and T. Suzuki.** 2008. Critical role of virion-associated cholesterol and sphingolipid in hepatitis C virus infection. J. Virol. **82:**5715–5724.
4. **Amemiya, F., S. Maekawa, Y. Itakura, A. Kanayama, A. Matsui, S. Takano, T. Yamaguchi, J. Itakura, T. Kitamura, T. Inoue, M. Sakamoto, K. Yamau-**

chi, S. Okada, A. Yamashita, N. Sakamoto, M. Itoh, and N. Enomoto. 2008. Targeting lipid metabolism in the treatment of hepatitis C virus infection. J. Infect. Dis. **197:**361–370.
5. **Binder, M., D. Quinkert, O. Bochkarova, R. Klein, N. Kezmic, R. Bartenschlager, and V. Lohmann.** 2007. Identification of determinants involved in initiation of hepatitis C virus RNA synthesis by using intergenotypic replicase chimeras. J. Virol. **81:**5270–5283.
6. **Biswal, B. K., M. M. Cherney, M. Wang, L. Chan, C. G. Yannopoulos, D. Bilimoria, O. Nicolas, J. Bedard, and M. N. James.** 2005. Crystal structures of the RNA-dependent RNA polymerase genotype 2a of hepatitis C virus reveal two conformations and suggest mechanisms of inhibition by non-nucleoside inhibitors. J. Biol. Chem. **280:**18202–18210.
7. **Blight, K. J., J. A. McKeating, J. Marcotrigiano, and C. M. Rice.** 2003. Efficient replication of hepatitis C virus genotype 1a RNAs in cell culture. J. Virol. **77:**3181–3190.
8. **Chamberlain, R. W., N. J. Adams, L. A. Taylor, P. Simmonds, and R. M. Elliott.** 1997. The complete coding sequence of hepatitis C virus genotype 5a, the predominant genotype in South Africa. Biochem. Biophys. Res. Commun. **236:**44–49.
9. **Chinnaswamy, S., I. Yarbrough, S. Palaninathan, C. T. Kumar, V. Vijayaraghavan, B. Demeler, S. M. Lemon, J. C. Sacchettini, and C. C. Kao.** 2008. A locking mechanism regulates RNA synthesis and host protein interaction by the hepatitis C virus polymerase. J. Biol. Chem. **283:**20535–20546.
10. **Chou, P. Y., and G. D. Fasman.** 1974. Prediction of protein conformation. Biochemistry **13:**222–245.
11. **Fujimoto, T., H. Kogo, K. Ishiguro, K. Tauchi, and R. Nomura.** 2001. Caveolin-2 is targeted to lipid droplets, a new "membrane domain" in the cell. J. Cell Biol. **152:**1079–1085.
12. **Gottwein, J. M., T. K. Scheel, B. Callendret, Y. P. Li, H. B. Eccleston, R. E. Engle, S. Govindarajan, W. Satterfield, R. H. Purcell, C. M. Walker, and J. Bukh.** Novel infectious cDNA clones of hepatitis C virus genotype 3a (strain S52) and 4a (strain ED43): genetic analyses and *in vivo* pathogenesis studies. J. Virol. **84:**5277–5293.
13. **Hammache, D., G. Pieroni, N. Yahi, O. Delezay, N. Koch, H. Lafont, C. Tamalet, and J. Fantini.** 1998. Specific interaction of HIV-1 and HIV-2 surface envelope glycoproteins with monolayers of galactosylceramide and ganglioside GM3. J. Biol. Chem. **273:**7967–7971.
14. **Hang, J. Q., Y. Yang, S. F. Harris, V. Leveque, H. J. Whittington, S. Rajyaguru, G. Ao-Ieong, M. F. McCown, A. Wong, A. M. Giannetti, S. Le Pogam, F. Talamas, N. Cammack, I. Najera, and K. Klumpp.** 2009. Slow binding inhibition and mechanism of resistance of non-nucleoside polymerase inhibitors of hepatitis C virus. J. Biol. Chem. **284:**15517–15529.
15. **Huang, H., F. Sun, D. M. Owen, W. Li, Y. Chen, M. Gale, Jr., and J. Ye.** 2007. Hepatitis C virus production by human hepatocytes dependent on assembly and secretion of very low-density lipoproteins. Proc. Natl. Acad. Sci. U. S. A. **104:**5848–5853.
16. **Ishii, N., K. Watashi, T. Hishiki, K. Goto, D. Inoue, M. Hijikata, T. Wakita, N. Kato, and K. Shimotohno.** 2006. Diverse effects of cyclosporine on hepatitis C virus strain replication. J. Virol. **80:**4510–4520.
17. **Kashiwagi, T., K. Hara, M. Kohara, K. Kohara, J. Iwahashi, N. Hamada, H. Yoshino, and T. Toyoda.** 2002. Kinetic analysis of C-terminally truncated RNA-dependent RNA polymerase of hepatitis C virus. Biochem. Biophys. Res. Commun. **290:**1188–1194.
18. **Kato, T., T. Date, M. Miyamoto, A. Furusaka, K. Tokushige, M. Mizokami, and T. Wakita.** 2003. Efficient replication of the genotype 2a hepatitis C virus subgenomic replicon. Gastroenterology **125:**1808–1817.
19. **Kiyosawa, K., T. Sodeyama, E. Tanaka, Y. Gibo, K. Yoshizawa, Y. Nakano, S. Furuta, Y. Akahane, K. Nishioka, R. H. Purcell, et al.** 1990. Interrelationship of blood transfusion, non-A, non-B hepatitis and hepatocellular carcinoma: analysis by detection of antibody to hepatitis C virus. Hepatology **12:**671–675.
20. **Lambot, M., S. Fretier, A. Op De Beeck, B. Quatannens, S. Lestavel, V. Clavey, and J. Dubuisson.** 2002. Reconstitution of hepatitis C virus envelope glycoproteins into liposomes as a surrogate model to study virus attachment. J. Biol. Chem. **277:**20625–20630.
21. **Lemon, S., C. Walker, M. Alter, and M. Yi.** 2007. Hepatitis C virus, p. 1253–1304. *In* D. M. Knipe, P. M. Howley, D. E. Griffin, R. A. Lamb, M. A. Martin, B. Roizman, and S. E. Straus (ed.), Fields virology, 5th ed. Lippincott Williams & Wilkins, Philadelphia, PA.
22. **Mahfoud, R., N. Garmy, M. Maresca, N. Yahi, A. Puigserver, and J. Fantini.** 2002. Identification of a common sphingolipid-binding domain in Alzheimer, prion, and HIV-1 proteins. J. Biol. Chem. **277:**11292–11296.
23. **Miyake, Y., Y. Kozutsumi, S. Nakamura, T. Fujita, and T. Kawasaki.** 1995. Serine palmitoyltransferase is the primary target of a sphingosine-like immunosuppressant, ISP-1/myriocin. Biochem. Biophys. Res. Commun. **211:**396–403.
24. **Miyanari, Y., K. Atsuzawa, N. Usuda, K. Watashi, T. Hishiki, M. Zayas, R. Bartenschlager, T. Wakita, M. Hijikata, and K. Shimotohno.** 2007. The lipid droplet is an important organelle for hepatitis C virus production. Nat. Cell Biol. **9:**1089–1097.
25. **Murayama, A., T. Date, K. Morikawa, D. Akazawa, M. Miyamoto, M. Kaga, K. Ishii, T. Suzuki, T. Kato, M. Mizokami, and T. Wakita.** 2007. The NS3 helicase and NS5B-to-3′X regions are important for efficient hepatitis C virus strain JFH-1 replication in Huh7 cells. J. Virol. **81:**8030–8040.
26. **Murayama, A., L. Weng, T. Date, D. Akazawa, X. Tian, T. Suzuki, T. Kato, Y. Tanaka, M. Mizokami, T. Wakita, and T. Toyoda.** 2010. RNA polymerase activity and specific RNA structure are required for efficient HCV replication in cultured cells. PLoS Pathog. **6:**e1000885.
27. **Ostermeyer, A. G., J. M. Paci, Y. Zeng, D. M. Lublin, S. Munro, and D. A. Brown.** 2001. Accumulation of caveolin in the endoplasmic reticulum redirects the protein to lipid storage droplets. J. Cell Biol. **152:**1071–1078.
28. **Saito, I., T. Miyamura, A. Ohbayashi, H. Harada, T. Katayama, S. Kikuchi, Y. Watanabe, S. Koi, M. Onji, Y. Ohta, et al.** 1990. Hepatitis C virus infection is associated with the development of hepatocellular carcinoma. Proc. Natl. Acad. Sci. U. S. A. **87:**6547–6549.
29. **Sakamoto, H., K. Okamoto, M. Aoki, H. Kato, A. Katsume, A. Ohta, T. Tsukuda, N. Shimma, Y. Aoki, M. Arisawa, M. Kohara, and M. Sudoh.** 2005. Host sphingolipid biosynthesis as a target for hepatitis C virus therapy. Nat. Chem. Biol. **1:**333–337.
30. **Shi, S. T., K. J. Lee, H. Aizaki, S. B. Hwang, and M. M. Lai.** 2003. Hepatitis C virus RNA replication occurs on a detergent-resistant membrane that cofractionates with caveolin-2. J. Virol. **77:**4160–4168.
31. **Simister, P., M. Schmitt, M. Geitmann, O. Wicht, U. H. Danielson, R. Klein, S. Bressanelli, and V. Lohmann.** 2009. Structural and functional analysis of hepatitis C virus strain JFH1 polymerase. J. Virol. **83:**11926–11939.
32. **Tsukiyama-Kohara, K., S. Tone, I. Maruyama, K. Inoue, A. Katsume, H. Nuriya, H. Ohmori, J. Ohkawa, K. Taira, Y. Hoshikawa, F. Shibasaki, M. Reth, Y. Minatogawa, and M. Kohara.** 2004. Activation of the CKI-CDK-Rb-E2F pathway in full genome hepatitis C virus-expressing cells. J. Biol. Chem. **279:**14531–14541.
33. **Umehara, T., M. Sudoh, F. Yasui, C. Matsuda, Y. Hayashi, K. Chayama, and M. Kohara.** 2006. Serine palmitoyltransferase inhibitor suppresses HCV replication in a mouse model. Biochem. Biophys. Res. Commun. **346:**67–73.
34. **Wasley, A., and M. J. Alter.** 2000. Epidemiology of hepatitis C: geographic differences and temporal trends. Semin. Liver Dis. **20:**1–16.
35. **Watashi, K., N. Ishii, M. Hijikata, D. Inoue, T. Murata, Y. Miyanari, and K. Shimotohno.** 2005. Cyclophilin B is a functional regulator of hepatitis C virus RNA polymerase. Mol. Cell **19:**111–122.
36. **Weng, L., J. Du, J. Zhou, J. Ding, T. Wakita, M. Kohara, and T. Toyoda.** 2009. Modification of hepatitis C virus 1b RNA polymerase to make a highly active JFH1-type polymerase by mutation of the thumb domain. Arch. Virol. **154:**765–773.
37. **Yasuda, S., H. Kitagawa, M. Ueno, H. Ishitani, M. Fukasawa, M. Nishijima, S. Kobayashi, and K. Hanada.** 2001. A novel inhibitor of ceramide trafficking from the endoplasmic reticulum to the site of sphingomyelin synthesis. J. Biol. Chem. **276:**43994–44002.
38. **Zhong, J., P. Gastaminza, G. Cheng, S. Kapadia, T. Kato, D. R. Burton, S. F. Wieland, S. L. Uprichard, T. Wakita, and F. V. Chisari.** 2005. Robust hepatitis C virus infection in vitro. Proc. Natl. Acad. Sci. U. S. A. **102:**9294–9299.

Organic & Biomolecular Chemistry

Dynamic Article Links
View Article Online

Cite this: *Org. Biomol. Chem.*, 2012, **10**, 5783

www.rsc.org/obc

COMMUNICATION

Selective thioether macrocyclization of peptides having the N-terminal 2-chloroacetyl group and competing two or three cysteine residues in translation†‡

Kazuhiro Iwasaki,[a] Yuki Goto,[b] Takayuki Katoh[b] and Hiroaki Suga*[b]

Received 11th February 2012, Accepted 29th February 2012
DOI: 10.1039/c2ob25306b

The mode of thioether macrocyclization of peptides containing an N-terminal 2-chloroacetyl group and two or three competing cysteine residues at downstream positions has been extensively studied, leading to a strategy for designated formation of overlapping-bicyclic peptides or dumbbell-type bicyclic peptides.

Naturally occurring peptides isolated from various organisms often have macrocyclic structures.[1] These structural features rigidify their tertiary structure, often granting them high affinities to the binding partners or targets. Unlike inter-sidechain disulfide bonds mostly found in ribosomally synthesized proteins, macrocyclization in such peptides takes place in various ways, *i.e.* head-to-tail, head-to-sidechain, sidechain-to-tail, inter-sidechain and their combinations,[2] giving not only their structural diversities but also greater physiological stability.[3] Since the formation of these unique bonds does not occur spontaneously, post-translational modification enzymes or enzymes in a part of non-ribosomal peptide synthetase are involved in the transformation.[4] On the other hand, as such enzymes generally have a preference toward certain sets of peptide sequences and/or particular recognition motifs upstream and/or downstream of the target sequences, their versatility for the synthesis of diverse and artificial macrocyclic peptides could be limited.

To circumvent this limitation, we recently devised a methodology[5] for spontaneous thioether macrocyclization of ribosomally expressed peptides using Flexible *In-vitro* Translation (FIT) system.[6] In this system, an artificial amino acid bearing a 2-chloroacetyl (ClAc) group on the α-amino group was incorporated by initiation codon reprogramming at the N-terminus, and reacts with sulfhydryl group in a cysteine (C) residue at a downstream position (Fig. 1a). Although this head-to-sidechain macrocyclization chemistry itself has been known for the chemical synthesis of peptides,[7] the above method using the FIT system represents the first example of thioether macrocyclization of ribosomally expressed peptides. Most importantly, this methodology allows us to readily construct various sequences and lengths of thioether macrocyclic peptides by simply designing their mRNA sequences which are transcribed from the corresponding synthetic DNAs *in vitro*.[5] Moreover, we have recently constructed such genetically encoded libraries of thioether macrocyclic peptides with a complexity of over 10^{12} and applied them to the discovery of inhibitors against various enzyme targets, *e.g.* E6AP,[8] Akt2,[9] SIRT2,[10] by integration with the mRNA display technique,[11] referred to as RaPID (Random non-standard Peptide Integrated Discovery) system as a whole.

A typical design of the above libraries is to have an *N*-ClAc-amino acid encoded by AUG as an initiator, random elongator amino acid sequences encoded by $(NNK)_n$ (K = U or G, n = 7–15), $(NNU)_n$, or $(NNC)_n$, followed by a cysteine (C) encoded

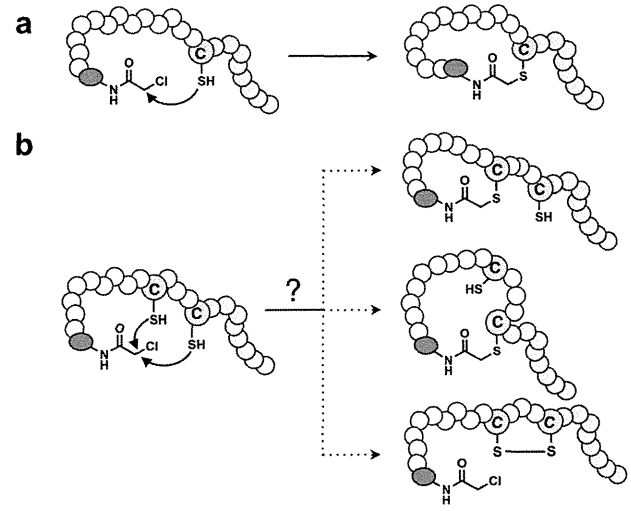

Fig. 1 Schematic representation of peptide macrocyclization closed by a thioether bond. (**a**) Peptide with N-terminal ClAc group that reacts with a cysteine (C) residue. (**b**) Three possible cyclization pathways in *N*-ClAc-peptides with two cysteine residues.

[a]*Department of Chemistry and Biotechnology, Graduate School of Engineering, the University of Tokyo, 7-3-1 Hongo, Bunkyo-ku, Tokyo 113-8656, Japan*
[b]*Department of Chemistry, Graduate School of Science, the University of Tokyo, 7-3-1 Hongo, Bunkyo-ku, Tokyo 113-8654, Japan. E-mail: hsuga@chem.s.u-tokyo.ac.jp*

†This article is part of the *Organic & Biomolecular Chemistry* 10th Anniversary issue.

‡Electronic supplementary information (ESI) available: Materials, Experimental procedures, MS data, and MS/MS data. See DOI: 10.1039/c2ob25306b

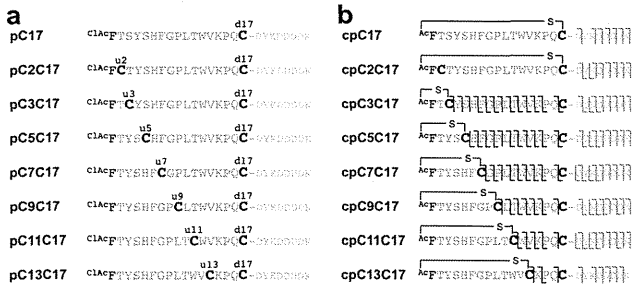

Fig. 2 Peptides and their fragmentation profiles observed in MALDI--TOF/TOF mass spectrometry. (**a**) Sequences of linear peptides expressed in this study. (**b**) Observed fragment peaks in each cyclized peptide and putative thioether bond formation based on the fragmentation profile. L shape and rotated L shape denote observations of y-ion and b-ion peaks, respectively.

by UGC. As a result, the major fraction of expressed peptides would cyclize between the N-terminus and the designated C residue at the C-terminus. However, during the course of such selection studies, we encountered active peptide sequences containing two (or possibly more) cysteine residues, one of which appeared in the random region encoded by UGU or UGC. In such peptides (Fig. 1b), both C residues could potentially react with the N-terminal ClAc group to form a thioether bond,[8] but it was unclear which bond would be preferentially or even selectively formed in such peptide sequences (Fig. 1b, top *vs.* middle). Alternatively, a disulfide bond between two C residues could possibly compete with the thioether bond formation (Fig. 1b, bottom). To understand a general rule of macrocyclization in such peptides, here we have designed experiments to express model peptides varying the position of an 'upstream Cys' (^{u}C) residue in addition to the designated 'downstream Cys' (^{d}C) residue.

We used a FIT system customized for the initiation codon reprogramming, where an initiator tRNA charged with *N*-ClAc-phenylalanine (^{ClAc}Phe) by means of flexizyme was supplemented to a Met-deficient cell-free translation system. We designed seven mRNA sequences encoding 25-mer model peptides (Fig. 2a), each of which was initiated with ^{ClAc}Phe, elongated with 15 residues containing ^{u}C and ^{d}C, and further elongated with a Flag tag (DYKDDDDK, where D, Y, K are aspartate, tyrosine, and lysine; it is used for not only an affinity purification tag but also for facilitating ionization of expressed peptides in mass spectrometry). In these peptides, ^{u}C was located in the 2nd position or an odd position from the 3rd to the 13th position along with a fixed ^{d}C at the 17th position (pC2C17–pC13C17, where the former and latter number denotes the position of ^{u}C and ^{d}C residue and p strands for peptide). Thus, each peptide would possibly produce three macrocyclic structures with a thioether bond between the N-terminus and ^{u}C or ^{d}C, or an ^{u}C–^{d}C disulfide bond. As a control, an mRNA sequence encoding a simple thioether macrocyclic peptide was also prepared (pC17).

All mRNA sequences expressed the encoded peptide with a loss of approximately 36 Da from the molecular mass of the full-length peptide, *i.e.* a loss of HCl, as a major product peak confirmed by MALDI-TOF (Fig. S1‡). This result indicated that the thioether bond formation preferentially occurred over the disulfide bond formation. The respective peptides were then subjected to the fragmentation by MALDI-TOF/TOF, of which the individual peaks were assigned to the expected fragments. Interestingly, two peptides, cpC17 and cpC2C17 (c stands for cyclic) were poorly fragmented at the region between F1 and ^{d}C17 (Fig. S2‡). On the other hand, cpC3C17–cpC13C17 afforded various peaks of fragments, supposedly originating from the linear region when macrocyclization took place between the N-terminus and ^{u}C; whereas, fragment of the thioether macrocyclic region was not found similar to that observed for cpC17 (Fig. S3‡). These results consistently suggested that macrocyclization of pC3C17–pC13C17 took place between the N-terminus and ^{u}C, giving the respective structures consisting of a macrocyclic head and a linear tail with a free sulfhydryl on ^{d}C17. In contrast, macrocyclization of pC2C17 predominantly took place between the N-terminus and ^{d}C17, giving the macrocyclic structure with a free sulfhydryl on ^{u}C2 (Fig. 2b). This selective macrocyclization could be attributed to the fact that the nucleophilic attack of the sulfhydryl group of ^{u}C2 on the α-carbon of the *N*-ClAc group required the formation of a constrained 9-membered ring, which might be unfavourable over macrocyclization between the N-terminus and ^{d}C17.

To solidify the above hypothesis, we expressed cpC3C17 peptide containing a single ester bond (cpC3e12C17; e denoting the ester bond) where tryptophan at the 12th position (W12) was replaced with phenyllactic acid (^{HO}F) by reprogramming of its codon (Fig. S4a‡).[12] As a control, we also expressed cpC17 with the same ester substitution at the 12th position (Fig. S4b‡). MALDI-TOF analysis of each peptide confirmed the production of macrocyclic peptide-ester hybrid as a single major product (Fig. S4c and d‡). Upon subjecting to alkaline hydrolysis, the ester bond was selectively cleaved to yield a product or products as follows: in cpC3e12C17, two fragment peaks were observed, each of which was assigned to the thioether macrocyclic peptide with the carboxylate tail (**1**) and the linear tail peptide (**2**) cleaved at ^{HO}F, respectively (Fig. S4c‡); in a control peptide cpe12C17, on the other hand, a single peak with the molecular weight corresponding to the hydrolysis product at the 12th position (**3**) was detected as a single piece of sequence (Fig. S4d‡). These results were consistent with our hypothesis that the macrocyclization of pC3C17–pC13C17 took place between the N-terminus and ^{u}C.

With all knowledge together, we designed bicyclic peptides consisting of a head-to-sidechain thioether bond and an inter-sidechain disulfide bond. We first demonstrated expression of a peptide, referred to as pC2C10C17, where leucine at the 10th position (L10) in pC2C17 was replaced with a 'middle Cys' (^{m}C10) residue. Because ^{u}C2 should not react with the N-terminal ClAc group, we expected that the sulfhydryl group of ^{m}C10 would spontaneously react with the N-terminus, leaving two thiol-free cysteine residues, ^{u}C2 and ^{d}C17; then these two residues would form a disulfide bond under mild oxidation conditions, yielding an overlapping-bicyclic backbone structure (Fig. 3a). In fact, the mass spectrum of the expressed pC2C10C17 after air-oxidization showed a peak corresponding to the expected bicyclic structure (Fig. 3b, pC2C10C17-oxi). Furthermore, the tandem mass analysis of cpC2C10C17-oxi by MALDI-TOF/TOF showed fragment peaks only corresponding

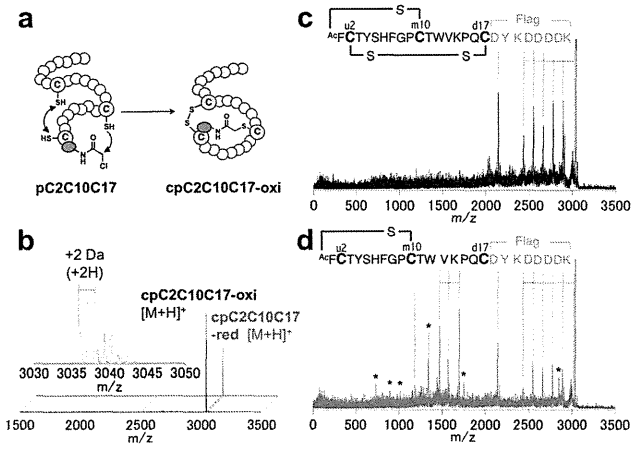

Fig. 3 Expression of an overlapping-bicyclic peptide consisting of a thioether bond and a disulfide bond. (a) Schematic representation of macrobicyclic peptides based on the pC2C10C17 scaffold. Because C2 is less susceptible to the reaction with the *N*-ClAc group, C10 predominantly forms a thioether bond and the remaining C2 and C17 form a disulfide bond. (b) MALDI-TOF spectra of cpC2C10C17 with two forms. Mild air-oxidation of the expressed peptide yielded the peptide, cpC2C10C17-oxi, that was consistent with the molecular mass containing a thioether bond and a disulfide bond (black spectrum). Its TCEP treatment yielded a mass with an additional 2 Da (cpC2C10C17-red), suggesting that the disulfide bond was reduced (red spectrum). The inset figure shows an expanded 3030–3050 *m/z* area of the superimposed spectra of cpC2C10C17-oxi (Cal. 3036.23, Obs. 3036.08) and cpC2C10C17-red (Cal. 3038.24, Obs. 3038.32). (c) MALDI-TOF/TOF spectrum of cpC2C10C17-oxi. (d) MALDI-TOF/TOF spectrum of cpC2C10C17-red. Assigned b-ion peaks are shown in the figure. Peaks labeled with asterisks are assigned as y-ion peaks.

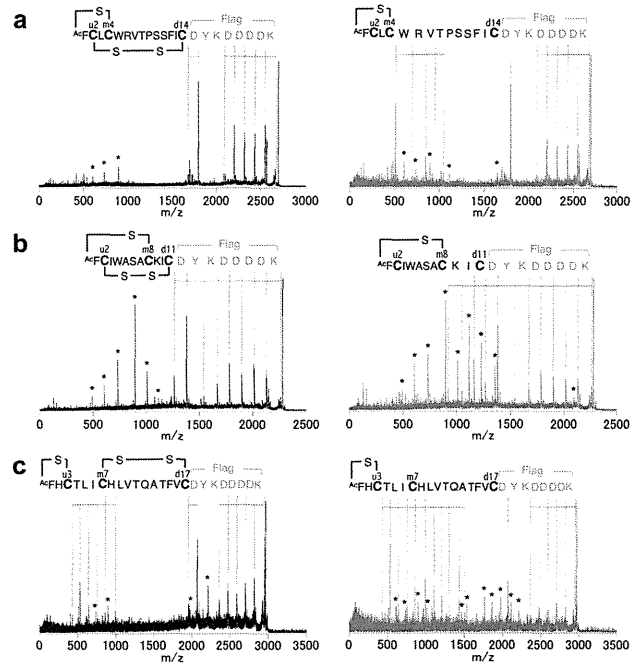

Fig. 4 MALDI-TOF/TOF spectra of overlapping- or dumbbell-type macrocyclic peptides. (a) cpC2C4C14, (b) cpC2C8C11, and (c) cpC3C7C17. Mild air-oxidation of the respective expressed peptide yielded the bicyclic structure that was consistent with the molecular mass containing a thioether bond and a disulfide bond (spectra of peptide-oxi shown in black). Upon treatment with TCEP, the molecular mass of each peptide-oxi increased by 2 Da, suggesting that the disulfide bond was reduced to yield monocyclic peptide (spectra of peptide-red shown in red). Assigned b-ion peaks are shown in the figure. Peaks labeled with asterisks are assigned as y-ion peaks.

to the linear Flag region (Fig. 3c), indicating that the desired overlapping-bicyclic structure was formed. Upon reduction treatment of pC2C10C17-oxi with tris(2-carboxyethyl)phosphine (TCEP), the molecular mass of pC2C10C17-oxi increased by approximately 2 Da, implying that the disulfide bond was reduced to form pC2C10C17-red (Fig. 3b, pC2C10C17-red). Tandem mass analysis of pC2C10C17-red yielded additional peaks corresponding to some fragmentations in the region between ^{m}C10 and ^{d}C17 (Fig. 3d). This result gave solid evidence that the designed overlapping-bicyclic peptide consisting of the head-to-sidechain and inter-sidechain bonds was produced.

To demonstrate the designer generality of this approach, we also expressed ^{u}C2-peptides varying in the position of ^{m}CX (X = 4, 5, 6, or 8) in the combination of ^{d}CY (Y = 7, 10, 11, or 14) with arbitrary sequence compositions and lengths. In all cases, production of the desired bicyclic peptide was confirmed by MALDI-TOF/TOF (Fig. 4a for X = 4 and Y = 14, and b for X = 8 and Y = 11; see also Fig. S5a, b, c, and d‡ for other combinations). Moreover, ^{u}C3-peptides having two different positions of ^{m}CX (X = 7, and 13) were also expressed, yielding dumbbell-type peptides (Fig. 4c for X = 7; see also Fig. S5e‡ for X = 13). Taken together, this designer bicyclization strategy enables us to construct various bicyclic peptides with desired sequence compositions.

Conclusions

Here we have shown selective macrocyclization of peptides having the N-terminal ClAc group with two competing C residues expressed in translation machinery under the reprogrammed genetic code. The nearest ^{u}C (upstream C) residue generally dictates the spontaneous thioether bond formation *via* thiol-nucleophilic attack on the α-carbon of the ClAc group, thus forming a macrocyclic structure and leaving a ^{d}C (downstream C) residue unreacted. However, there is one exception where ^{u}C embedded at position 2 (^{u}C2) does not react with the ClAc group and instead ^{d}C residue predominantly reacts with the ClAc group, leaving the ^{u}C residue thiol-free. Based on this knowledge, we have devised a strategy for the synthesis of bicyclic peptides in which an additional middle C (^{m}C) residue between the ^{u}C2 and ^{d}C residues is embedded in the sequence, cyclizing the peptide by a thioether bond between ClAc and ^{m}C followed by a disulfide bond formation of ^{u}C2 and ^{d}C. This bicyclization is selective and fairly general independent of sequence compositions. Thus, this strategy is applicable for constructing a library consisting of such constrained bicyclic peptide scaffolds. Particularly, the integration of this library with RaPID system will allow us to rapidly select bicyclic peptides against a chosen protein target. This opens a new avenue to search a unique peptide 3-dimensional sequence space for bioactive peptides.

Acknowledgements

We thank H. Murakami for the discussion and development of the FIT system. This work was supported by a Grants-in-Aid of Japan Society for Promotion of Science (JSPS), the Specially Promoted Research (21000005) and the Industrial Science and Technology Program in the New Energy and Industrial Technology Development Organization to H.S.; Grants-in-Aid for JSPS Fellows (22–9695) to K.I.; Grants-in-Aid for Young Scientists (B) (22750145) from JSPS and PRESTO, Japan Science and Technology Agency (10206) to Y.G.; and Grants-in-Aid for Young Scientists (B) (22710210) from JSPS to T.K.

Notes and references

1 D. P. Fairlie, G. Abbenante and D. R. March, *Curr. Med. Chem.*, 1995, **2**, 654–686.

2 (*a*) A. Paladini and L. C. Craig, *J. Am. Chem. Soc.*, 1954, **76**, 688–692; (*b*) M. Dreyfuss, E. Harri, H. Hofmann, H. Kobel, W. Pache and H. Tscherter, *Eur. J. Appl. Microbiol.*, 1976, **3**, 125–133; (*c*) A. C. Whyte, B. K. Joshi, J. B. Gloer, D. T. Wicklow and P. F. Dowd, *J. Nat. Prod.*, 2000, **63**, 1006–1009; (*d*) T. Tanaka, E. Tsukuda, M. Nozawa, H. Nonaka, T. Ohno, H. Kase, K. Yamada and Y. Matsuda, *Mol. Pharmacol.*, 1994, **45**, 724–730; (*e*) B. A. Johnson, H. Anker and F. L. Meleney, *Science (Washington, D. C.)*, 1945, **102**, 376–377.

3 D. R. March, G. Abbenante, D. A. Bergman, R. I. Brinkworth, W. Wickramasinghe, J. Begun, J. L. Martin and D. P. Fairlie, *J. Am. Chem. Soc.*, 1996, **118**, 3375–3379.

4 (*a*) D. Schwarzer, R. Finking and M. A. Marahiel, *Nat. Prod. Rep.*, 2003, **20**, 275–287; (*b*) R. Finking and M. A. Marahiel, *Annu. Rev. Microbiol.*, 2004, **58**, 453–488; (*c*) M. A. Fischbach and C. T. Walsh, *Chem. Rev.*, 2006, **106**, 3468–3496.

5 Y. Goto, A. Ohta, Y. Sako, Y. Yamagishi, H. Murakami and H. Suga, *ACS Chem. Biol.*, 2008, **3**, 120–129.

6 (*a*) H. Murakami, A. Ohta, H. Ashigai and H. Suga, *Nat. Methods*, 2006, **3**, 357–359; (*b*) Y. Goto, T. Katoh and H. Suga, *Nat. Protocols*, 2011, **6**, 779–790.

7 (*a*) L. Yu, Y. H. Lai, J. V. Wade and S. M. Coutts, *Tetrahedron Lett.*, 1998, **39**, 6633–6636; (*b*) K. D. Roberts, J. N. Lambert, N. J. Ede and A. M. Bray, *Tetrahedron Lett.*, 1998, **39**, 8357–8360; (*c*) F. D. T. Lung, C. R. King and P. P. Roller, *Lett. Pept. Sci.*, 1999, **6**, 45–49; (*d*) S. C. Pero, L. Oligino, R. J. Daly, A. L. Soden, C. Liu, P. P. Roller, P. Li and D. N. Krag, *J. Biol. Chem.*, 2002, **277**, 11918–11926; (*e*) P. Li, M. L. Peach, M. C. Zhang, H. P. Liu, D. J. Yang, M. Nicklaus and P. P. Roller, *Bioorg. Med. Chem. Lett.*, 2003, **13**, 895–899; (*f*) F. M. Brunel and P. E. Dawson, *Chem. Commun.*, 2005, 2552–2554; (*g*) R. Tugyi, G. Mezo, E. Fellinger, D. Andreu and F. Hudecz, *J. Pept. Sci.*, 2005, **11**, 642–649; (*h*) K. D. Roberts, J. N. Lambert, J. Ede and A. M. Bray, *J. Pept. Sci.*, 2006, **12**, 525–532; (*i*) C. J. Porter and J. A. Wilce, *Biopolymers*, 2007, **88**, 174–181; (*j*) K. D. Roberts and N. J. Ede, *J. Pept. Sci.*, 2007, **13**, 811–821; (*k*) S. Jiang, C. Z. Liao, L. Bindu, B. L. Yin, K. W. Worthy, R. J. Fisher, T. R. Burke, M. C. Nicklaus and P. P. Roller, *Bioorg. Med. Chem. Lett.*, 2009, **19**, 2693–2698.

8 Y. Yamagishi, I. Shoji, S. Miyagawa, T. Kawakami, T. Katoh, Y. Goto and H. Suga, *Chem. Biol.*, 2011, **18**, 1562–1570.

9 Y. Hayashi, J. Morimoto and H. Suga, *ACS Chem. Biol.*, 2012, DOI: 10.1021/cb200388k.

10 J. Morimoto, Y. Hayashi and H. Suga, *Angew. Chem., Int. Ed. Engl.*, 2012, DOI: 10.1002/anie.201108118.

11 (*a*) R. W. Roberts and J. W. Szostak, *Proc. Natl. Acad. Sci. U. S. A.*, 1997, **94**, 12297–12302; (*b*) N. Nemoto, E. MiyamotoSato, Y. Husimi and H. Yanagawa, *FEBS Lett.*, 1997, **414**, 405–408.

12 (*a*) In addition to genetic code reprogramming, a hydroxy acid has been incorporated into amber codon in the following papers: A. Ohta, H. Murakami, E. Higashimura and H. Suga, *Chem. Biol.*, 2007, **14**, 1315–1322; (*b*) J. A. Ellman, D. Mendel and P. G. Schultz, *Science (Washington, D. C.)*, 1992, **255**, 197–200; (*c*) P. M. England, H. A. Lester and D. A. Dougherty, *Biochemistry*, 1999, **38**, 14409–14415; (*d*) S. W. Millward, T. T. Takahashi and R. W. Roberts, *J. Am. Chem. Soc.*, 2005, **127**, 14142–14143.

ACS chemical biology

Articles

pubs.acs.org/acschemicalbiology

In Vitro Selection of Anti-Akt2 Thioether-Macrocyclic Peptides Leading to Isoform-Selective Inhibitors

Yuuki Hayashi,[†] Jumpei Morimoto,[‡] and Hiroaki Suga*[,†]

[†]Department of Chemistry, Graduate School of Science and [‡]Department of Chemistry and Biotechnology, Graduate School of Engineering, The University of Tokyo, Tokyo, Japan

Supporting Information

ABSTRACT: The Akt kinase family, consisting of three isoforms in humans, is a well-validated class of drug target. Through various screening campaigns in academics and pharmaceutical industries, several promising inhibitors have been developed to date. However, due to the mechanistic and structural similarities of Akt kinases, it is yet a challenging task to discover selective inhibitors against a specific Akt isoform. We here report Akt-selective and also Akt2 isoform-selective inhibitors based on a thioether-macrocyclic peptide scaffold. Several anti-Akt2 peptides have been selected from a library by means of an *in vitro* display system, referred to as the RaPID (Random nonstandard Peptide Integrated Discovery) system. Remarkably, the majority of these "binding-active" anti-Akt2 peptides turned out to be "inhibitory active", exhibiting IC_{50} values of approximately 100 nM. Moreover, these peptides are not only selective to the Akt kinase family but also isoform-selective to Akt2. Particularly, one referred to as Pakti-L1 is able to discriminate Akt2 250- and 40-fold over Akt1 and Akt3, respectively. This proof-of-concept case study suggests that the RaPID system has a tremendous potential for the discovery of unique inhibitors with high family- and isoform-selectivity.

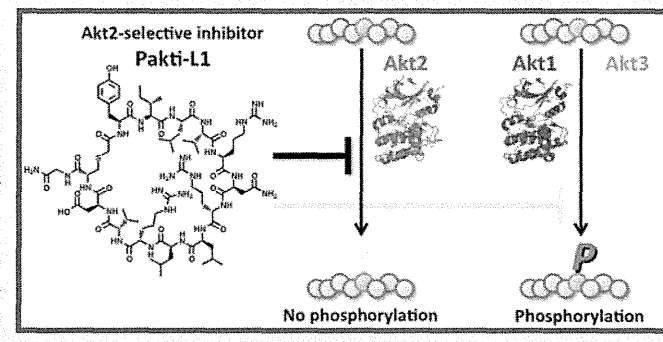

In human cells, the Akt family, belonging to the serine/threonine (S/T) kinase family, plays critical roles in regulating various signal transduction pathways.[1] Because misregulation of Akt causes alterations of apoptosis, cell proliferation, and metabolisms depending upon the Akt isoforms, it is of great interest for academics, as well as pharmaceutical industries, to develop inhibitors against this kinase family. Three isoforms, Akt1, Akt2, and Akt3, are known in the human Akt family. Akt1 activates the translocation of nuclear factors, such as NF-κB (nuclear factor of kappa light polypeptide gene enhancer in B-cells),[2] which suppress apoptosis in a transcription-independent manner; thereby it promotes cell survival. In fact, elevated expression and activation of Akt1 have been observed in human gastric, breast, prostate, and ovarian cancers, implying that it is a major factor in the cancer development, *i.e.*, Akt1 is an oncogene.[3,4] Similar events involving Akt2 have been also observed in various carcinomas,[5−7] consistent with a view that Akt2 plays a similar role as Akt1 in developing malignant phenotype of these cancers. However, data generated by experiments involving Akt1 or Akt2-deficient transgenic mice have suggested that Akt2 likely plays a specific role in the insulin receptor signal transduction, implying that Akt2 is an important drug target for controlling diabetes mellitus.[8] The function of Akt3 is least understood among the Akt family, but it is expressed predominantly in the brain.[9] Presumably, it contributes to the development of the brain through the activation of growth factor mediated signal transductions.[10]

Because of the therapeutic significance of Akt in cancers and other diseases, a number of screening campaigns of molecules have been conducted to yield potent Akt inhibitors (representative Akt inhibitors along with their potency and selectivity against a specific Akt isoform over other isoforms and kinase family are summarized in Supplementary Table 1). There are four classes of inhibitors: (I) those that compete for binding to the ATP-binding site, (II) those that bind to the pleckstrin homology domain (PH domain), (III) those that bind to an allosteric site(s), and (IV) those derived from substrate peptide sequences and others.

The class I inhibitors, represented by A674563 and GSK690693, have remarkable potencies against all Akt isoforms with low nanomolar IC_{50}'s.[11−15] However, since all kinase families have structurally similar ATP-binding sites, they generally show broad spectra of inhibitory activities against many S/T kinases with comparable potencies, thus interacting with various cellular kinases in a nonselective manner. On the other hand, since the PH domain of the Akt family is unique over other kinases, the class II inhibitors are inherently Akt-selective, but because all Akt members have nearly identical PH domains, they are so far unable to distinguish a specific isoform from other isoforms.[16−21] Representative class III inhibitors are

Received: September 23, 2011
Accepted: January 11, 2012
Published: January 24, 2012

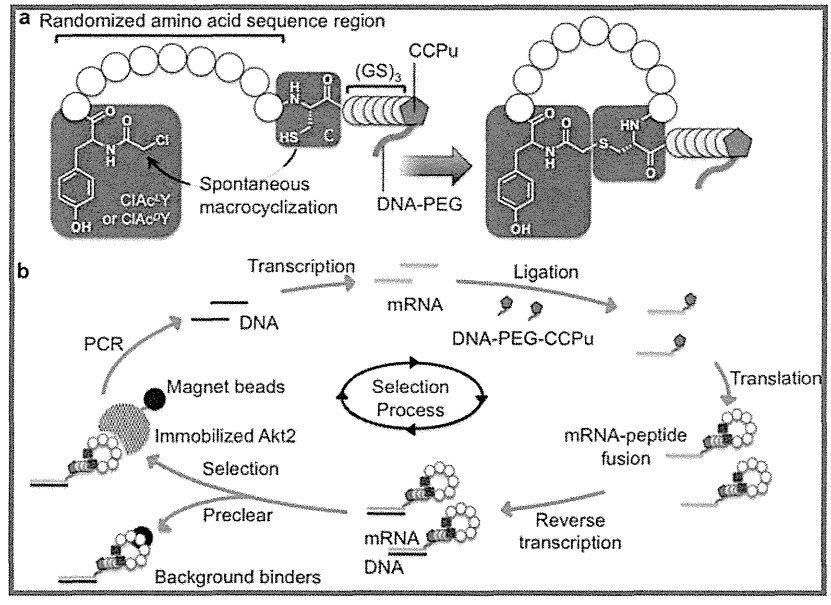

Figure 1. Schematic presentation of the macrocyclic peptide library and RaPID selection. (a) A macrocyclic peptide library closed by a thioether bond. The randomized amino acid sequence region (white circles) consists of 4–12 amino acid residues. Spontaneous cyclization takes place between $ClAc^{L}Y$ or $ClAc^{D}Y$ initiator and sulfhydryl group of a cysteine (C) residue, both shown in dark gray boxes. Although the C residue is designated right after the random region in each peptide, a C residue or residues can also be appeared from the random region to form a smaller ring sized head and a tail containing the unreacted cysteine residue(s). The $(GS)_3$-linker peptide is shown in gray circles. 5′-CCPu-3′ and DNA-PEG regions in DNA-PEG-CCPu are shown in a dark gray pentagon and a dark gray line, respectively. (b) Selection using RaPID system. DNA and RNA libraries are shown in black and gray lines, respectively. The full-length Akt2 protein and Ni^{2+}-NTA magnetic beads are shown in a black-dotted circle and black circles, respectively.

MK2206, Akti-1, Akti-2, and Akti-1/2 (Akt inhibitor VIII), all of which are categorized as allosteric inhibitors.[22−25] Among them, Akti-1/2 has been extensively studied by the X-ray structure complexed with Akt1.[26] This inhibitor binds to the interface between "N-lobe" and "C-lobe" in the kinase domain and further interacts with the PH domain, resulting in stabilization of the ternary interactions. This ternary complex, referred to as a "PH-in" form, prevents phosphorylation of T308 and S473, inhibiting activation of the kinase domain. The IC_{50} value of Akti-1/2 is 58 nM against Akt1 compared with 4- and 40-fold elevated IC_{50} values against Akt2 and Akt3, respectively. On the other hand, Akti-2, which is structurally similar to Akti-1/2, exhibits a greater isoform-selectivity (70-fold against Akt1 over Akt2), but its potency dropped to 325 nM IC_{50}. The class IV inhibitors competitively bind to the protein substrate-binding site of Akt.[27−30] Although the isoform selectivity of this class of inhibitors is unknown in literature, they display marginal inhibitory potencies even *in vitro*.

Even though simultaneous inhibition of all members of the Akt family by ATP-competitive inhibitors gave a maximal efficacy for caspase-3/7 activation,[31] these inhibitors may have a risk of side effects caused by undesired inhibitions of non-Akt kinases. An approach to devise inhibitors binding to the PH domain has yielded Akt-selective inhibitors, but it has been yet difficult to install an isoform-selectivity into the inhibitors. Allosteric inhibitors have given the Akt- and isoform-selective properties, but it remains difficult to achieve high selectivity and potency simultaneously against a specific isoform. Therefore, it is still a difficult challenge to devise Akt- and isoform-selective inhibitors.

We here report a potent Akt2 isoform-selective inhibitor with a 100 nM IC_{50} discovered from a library of thioether-macrocyclic peptides with a complexity of 10^{12}, by means of an *in vitro* display system, referred to as RaPID (Random nonstandard Peptide Integrated Discovery) system (Yamagishi *et al. Chem. Biol.*, in press).

RESULTS AND DISCUSSION

Thioether-Macrocyclic Peptide Libraries. In 2008, we reported a new strategy to ribosomally express thioether-macrocyclic peptides involving an initiation codon reprogramming. To facilitate such a codon reprogramming for this study, we have devised a FIT (Flexible In vitro Translation) system where a custom-made *in vitro* translation system lacking methionine (M) is supplied with *N*-(2-chloroacetyl)-aminoacyl-$tRNA^{fMet}_{CAU}$ (ClAc-aa-$tRNA^{fMet}_{CAU}$) prepared by a flexizyme (flexible tRNA acylation ribozyme),[32−35] resulting in a reassignment of AUG initiator codon from M to the ClAc-aa. In this setup, the peptide translation of mRNA is initiated by the ClAc-aa, and a cysteine (C) residue installed at a downstream position in the sequence reacts with the 2-chloroacetyl group, giving macrocyclic peptide closed by a thioether bond (Figure 1a).[36,37] The cyclization takes place spontaneously without an additional reagent, yielding a clean desired product almost regardless of the length and sequence composition. In fact, we were able to prepare a macrocyclic peptide library with various lengths from random sequences of mRNAs.

In the present work, we constructed two thioether-macrocyclic peptide libraries initiated by either L or D isomers of *N*-(2-chloroacetyl)-tyrosine ($ClAc^{L}Y$ or $ClAc^{D}Y$, respectively). To construct each peptide library, mRNA template libraries were designed to have AUG-$(NNK)_n$-UGC, where AUG and UGC assign $ClAc^{L}Y$ or $ClAc^{D}Y$ and C, respectively, which would undergo the thioether bond formation for cyclization; also where $(NNK)_n$ (N and K represent any of four bases and U or G, respectively) assign all possible 20 amino acids with a range of lengths between 4 and 12, *i.e.*, a mixture of peptides with a

Table 1. Selected Peptides with Frequency of Appearance and Their IC_{50} Values against Akt Isoforms[b]

Peptide	Sequence	Frequency	IC_{50} [nM]		
			Akt2	Akt1	Akt3
Pakti-L1	Ac-^{L}YILVRNRLLRVDCG-NH_2	28/37	110	>25,000	4,200
Pakti-L2	Ac-^{L}YWILITWPLVRRKCG-NH_2	2/37	120	~1,000[a]	~1,000[a]
Pakti-L3	Ac-^{L}YWIVLTWPIVTRRCG-NH_2	2/37	92	~1,000[a]	~1,000[a]
Pakti-L4	Ac-^{L}YTYWFVSMICG-NH_2	1/37	inactive	N.D.	N.D.
Pakti-L5	Ac-^{L}YIRRPWVPIMYLGCG-NH_2	3/37	active	N.D.	N.D.
Pakti-L6	Ac-^{L}YILVRNRPLRVDCG-NH_2	1/37	active	N.D.	N.D.
Pakti-D1	Ac-^{D}YAVRILGHYLQVGCG-NH_2	35/37	active	N.D.	N.D.
Pakti-D2	Ac-^{D}YLSRRHGLLFLIRCG-NH_2	1/37	inactive	N.D.	N.D.
Pakti-D3	Ac-^{D}YLSREFNLLFLVRCG-NH_2	1/37	active	N.D.	N.D.

[a] IC_{50} values were estimated by the graph shown in Figure.2b and c [b] Peptides shown in this table were synthesized by standard solid-phase synthesis and applied to the inhibition assay of kinase activities. IC_{50} values were determined by the plot shown in Figure 3. Pakti-L5, L6, D1, and D3 inhibited Akt2 kinase activity (the accurate IC_{50} value was undetermined), whereas Pakti-L4 and D2 were inactive by a preliminary assay. N.D. denotes "not determined" in this study.

random region of these lengths would be expressed. It should be noted that the thioether-macrocyclic peptide library initiated with ClAc^{D}Y would cover different conformational sequence space from that initiated with ClAc^{L}Y since a single D-isomer in the macrocyclic scaffold would potentially alter the tertiary structural conformers from those in all-L-macrocyclic peptides. We referred the respective libraries to as ^{L}Y- and ^{D}Y-libraries for our convenience in discussion below.

To perform the selection of active species, these libraries were integrated with an *in vitro* display method, so-called mRNA display,[38,39] where puromycin (Pu) was ligated to the 3′-end of a synthetic hybrid oligonucleotide (DNA-PEG-CCPu; the DNA sequence is complementary to the 3′-end sequence of mRNA, followed by a poly(ethylene glycol) linker, deoxyribonucleotides CC, and puromycin), which allows for fusion with the peptide C-terminus (Supplementary Table 2). To facilitate the integration, we designed the above mRNA libraries to have three repeats of (GGC)(AGC) encoding $(GS)_3$ (G, glycine; S, serine) after UGC (encoding a cysteine residue), UAG stop codon, followed by a short stretch of RNA that hybridizes the DNA-PEG-CCPu. It should be noted that our FIT system using this display experiment did not contain release factor-1 (RF1), which usually terminates the elongation at UAG stop codon; instead, ribosome would be stalled at UAG codon and the efficiency of puromycin-peptide fusion should be enhanced. By means of this system, the estimated complexity generated by the $(NNK)_n$ library transcribed from the corresponding DNA library was approximately 10^{14}, and the efficiency of the peptide-puromycin fusion was generally more than 30% in our hands for representative model peptides with the range of lengths and degenerated sequences used in the library (data not shown). Therefore, we confidently estimated the diversity of the initial display library to be 10^{12} or more. We referred to this system enabling display of nonstandard macrocyclic peptide libraries as the RaPID (Random nonstandard Peptide Integrated Discovery) system (Yamagishi *et al. Chem. Biol.*, in press). Significantly, the C-terminal end of each thioether-macrocyclic peptide in the library is covalently linked to its encoding mRNA *via* Pu, and thus active species of peptide based on their binding capability against a therapeutic target could be enriched by RT-PCR (reverse transcription polymerase chain reaction). Therefore, the RaPID selection process can be repeated until an active population emerges in the selected pool.

Selection of Anti-Akt2 Macrocyclic Peptides. We performed *in vitro* selection of the nonstandard macrocyclic peptides against Akt2 (Figure 1b). The ^{L}Y- and ^{D}Y-libraries were independently applied to the RaPID selection against a full-length Akt2 that was immobilized on Ni^{2+}-NTA magnetic beads *via* the interaction with hexa-His residues at the Akt2's N-terminus. Prior to the selection against Akt2-beads, the respective libraries were treated with the Ni^{2+}-NTA magnetic beads (up to 12 times) to remove undesired background-binding peptide species in the pool, and the peptide fraction unbound to the beads was then applied to the selection against Akt2-immobilized beads. At the sixth round, we observed an appreciable enrichment of active population in the both pools monitored by the recovery amount of selected cDNA by RT-PCR, while the background binding to the beads was significantly suppressed (Supplementary Figure 1).

The enriched pool was cloned and individual colonies were arbitrarily picked for sequencing, yielding a total of 37 DNA sequences from each of the ^{L}Y- and ^{D}Y-libraries (Table 1). The most abundant ^{L}Y-clone, referred to as Pakti-L1, was found 28 times in 37 clones, and shared the common sequence with Pakti-L6 found once. Pakti-L1 consists of 11 residues originating from the random sequence region, giving a total body length of a 13-mer macrocyclic peptide without the linker peptide region. Two clones, Pakti-L2 and 3, were each found twice, and shared a common sequence motif, consisting of 12 residues originating from the random region (a total of 14-mer body length). Pakti-L4 and L5 were independently found once and thrice, respectively. On the other hand, the ^{D}Y-library was dominated by a single kind of a peptide; Pakti-D1 was found 35 times. Pakti-D2 and D3 were found once, respectively, and shared the common sequence motif. Interestingly, no Pakti-D peptides had sequence similarity to any Pakti-L peptides. This implied that, even though the random region originated from

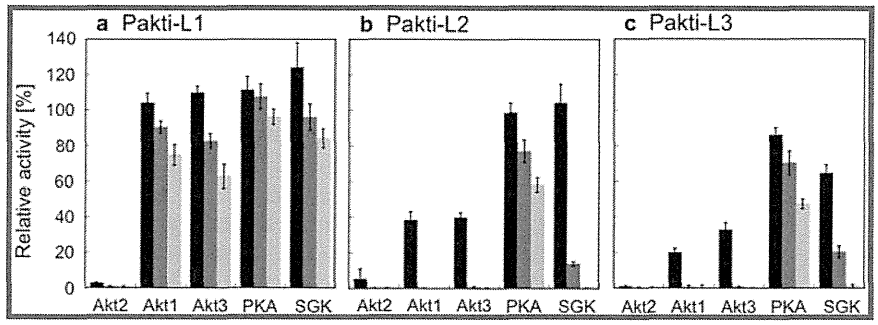

Figure 2. Inhibitory activities of Pakti-L1–L3 (a–c) against Akt isoforms and other kinases. (a) Akt- and isoform-selectivity of Pakti-L1. Black, gray, and light gray bars show observed activities of the kinase at the peptide concentrations of 1, 5, and 10 μM, respectively. The respective activity was defined as an average of activities of the kinase in triplicate in the presence of inhibitor relative to those in the absence of inhibitor. Error bars are shown as the standard deviations of the relative activities in triplicate. (b) Akt- and isoform-selectivity of Pakti-L2. (c) Akt- and isoform-selectivity of Pakti-L3.

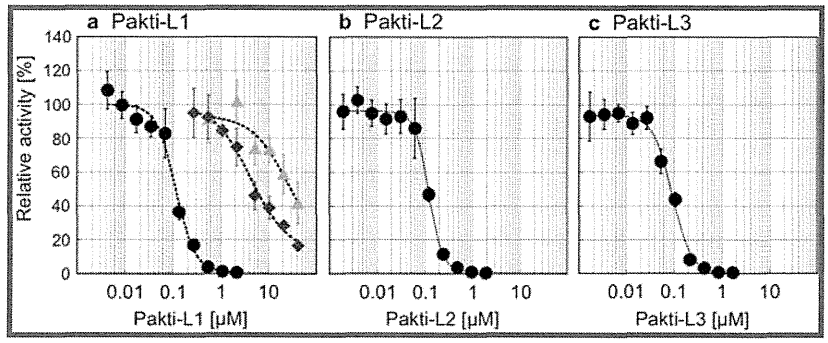

Figure 3. Titration of kinase activities as a function of Pakti-L inhibitor concentrations. (a) Inhibitory titration of Pakti-L1. Data plot in black circles are against Akt2. Those in light gray triangles and gray diamonds are against Akt1 and Akt3, respectively. IC_{50} values were determined by a curve fitting to a Hill equation generated by KaleidaGraph (Hulinks Inc.). (b) Inhibitory titration of Pakti-L2. (c) Inhibitory titration of Pakti-L3.

the same pool of mRNA sequences, the library composed of ^{L}Y-initiator covered different conformational sequence space from that of ^{D}Y-initiator.

Anti-Akt2 Macrocyclic Peptides Are Inhibitory Active. All peptides from the Pakti-L and -D families were chemically synthesized using a standard solid-phase method with an additional glycine-carboxamide at the C-terminus. The individual peptides were then subjected to kinase inhibitory screening using a universal S/T kinase assay system composed of biotin-labeled peptide substrates (HTRF KinEASE STK2 and STK3, the appropriate one of which was treated with the corresponding kinase). After the phosphorylation, the biotin in the substrate was captured with XL665-labeled streptavidin, and a phospho-specific monoclonal antibody labeled with Eu^{3+}-cryptate was used to detect the signal of time-resolved-fluorescence resonance energy transfer (TR-FRET). In this study, we used enzymatically active GST-Akt#-ΔPH (Carna Biosciences Inc.) in which GST, #, and ΔPH denoted glutathione *S*-transferase as a N-terminal tag, isoform number, and deletion of PH domain, respectively, and the respective Akt isoforms were phosphorylated at threonine/serine residues essential for the activation of kinase domain. Our preliminary activity screening for inhibition using Pakti-L1–L6 and Pakti-D1–D3 revealed that the Pakti peptides isolated in this study, except for Pakti-L4 and D2, were active inhibitors against Akt2 (Table 1). On the basis of this preliminary data, we chose three peptides from the Pakti-L family, Pakti-L1–L3, for further isoform-selectivity studies. In parallel, other representative S/T kinases, PKA (protein kinase A) and SGK (serum- and glucocorticoid-regulated protein kinase), were also tested for inhibition by these peptides (Figure 2a–c).

Akt- and Isoform-Selectivity of Pakti-L Peptides. The concentrations of each peptide were set at 1, 5, and 10 μM for the inhibitory test against Akt1–3, PKA, and SGK. Remarkably, under any of the above concentrations, Pakti-L1 completely shut down the kinase activity of Akt2, but all other kinases tested in this study retained activity over 50% even at 10 μM (Figure 2a). This result clearly shows a high isoform selectivity of Pakti-L1. Likewise, Pakti-L2 and L3 shut down the kinase activity of Akt2, but they also inhibited the kinase activity of both Akt1 and Akt3 to some extent (Figure 2b and c); at their 1 μM concentration, both Akt's gave an approximately 40% activity, and thus their IC_{50} values were estimated to be ~1 μM (Table 1). Similar to Pakti-L1, Pakti-L2 and L3 displayed very weak inhibitory activities against PKA and SGK (IC_{50} values could be <10 μM). Thus, Pakti-L2 and L3 are Akt2-selective but less isoform- and Akt-selective compared with Pakti-L1. Even though the *in vitro* selection of nonstandard macrocyclic peptides against Akt2 from the ^{L}Y- and ^{D}Y-libraries was based on their binding ability leading to enrichment, it has successfully yielded potent inhibitors from both libraries.

To assess more accurate IC_{50} values of the Akt2-inhibitors, we directly monitored the kinase activity of Akt2 by a classical filter-binding assay of ^{32}P-phosphorylated substrate peptide on a phosphocellulose paper.[40] For this experiment, we modified a known cross-reactive substrate, so-called crosstide, to generate a crosstide-KK in which two additional lysine residues were added to its C-terminus.[40,41] The phosphorylation activity was titrated in the presence of various concentrations of each peptide ranging from 2 to 2,100 nM against Akt2 (Figure 3a–c). All Pakti-L1–L3 displayed nearly the same inhibitory potencies against Akt2 with IC_{50} values of 100 nM (Table 1).

Because Pakti-L1 appears to exhibit a high selectivity to Akt2 according to the screening result (Figure 2a), we also attempted to determine the IC_{50} values against Akt1 and Akt3 (Figure 3a). The titration of Pakti-L1 in a range of 270−42,000 nM against Akt1 and Akt3 has revealed estimated IC_{50} values of 25 and 4.2 μM (Figure 3a and Table 1). It should be noted that the inhibitory activities of Pakti-L1 against Akt1 and Akt3 were intrinsically very weak, and therefore we were unable to completely titrate the inhibitory activity with 42 μM Pakti-L1, meaning that the above IC_{50} values were yet estimates. Nevertheless, the isoform selectivity of Pakti-L1 to Akt2 over Akt1 and Akt3 was 250- and 40-fold, respectively.

In summary, Pakti-L1, generated from ^{L}Y-library and studied in depth in the present work, displays an isoform-selective inhibitory activity against Akt2 over Akt1 and Akt3. It also exhibits nearly no activity against other families of S/T kinases. Thus, Pakti-L1 is a remarkable Akt-selective and Akt2 isoform-selective inhibitor. The other class of thioether-macrocyclic peptides, Pakti-L2 and L3, display potent inhibitory activity against Akt2, modest activities against Akt1/3, and very weak activity against other families of S/T kinases. Although they are weakly isoform-selective, they are highly Akt-selective inhibitors.

Discussion. The full-length of Akt2 used for the selection was an enzymatically inactive construct, *i.e.*, a nonphosphorylated form. Therefore, it is quite surprising that the majority of selected peptides found in ^{L}Y-library were able to show inhibitory potencies with a range of 100 nM IC_{50} against active Akt2. Moreover, all inhibitors found in this study inhibit the kinase activity of Akt2-ΔPH, suggesting that their binding site(s) should reside in the kinase domain of Akt2. The most intriguing question is how these macrocyclic peptides inhibit the kinase activity of Akt. Particularly, Pakti-L1 exhibits a high isoform-selective activity, so the questions where it binds in the Akt kinase domain and how it discriminates Akt2 over Akt1/3 are of greatest interest.

Since we have tertiary structural information of neither Pakti-L1 nor its complex with Akt2, we are only able to provide a speculative discussion for possible mechanisms of its isoform-selectivity, but it would be worthy to discuss such at this point. We propose two hypotheses as follows. The first hypothesis is that Pakti-L1 interacts with the substrate-binding domain and competitively inhibits Akt2 activity. It is known that a generic substrate sequence, such as crosstide, contains a RXRXX(S/T) motif (the phosphorylating S/T is assigned to position 0, and its N-terminal region is assigned to −1 to −5) where the arginine residues at positions −3 and −5, interact with the conserved glutamate residues (E236, E279, and E342) in Akt (Supplementary Figure 2a).[42] It turns out that Pakti-L1 has a RNR motif embedded in the middle of sequence (Table 1), and therefore this motif may be able to position Pakti-L1 into the active site. On the other hand, all Akt kinases share the same amino acid residues that interact with the substrate backbone amides or side chains, and unique residues in Akt2 differing from those in Akt1/3 are scattered outside of active site in the structure (see Supplementary Figure 2b). Therefore, if this hypothesis were correct, Pakti-L1 could use a unique mechanism, such as induced fit, to gain specific interactions, enabling the discrimination of Akt2 against Akt1/3.

The second hypothesis is that Pakti-L1 acts as an allosteric inhibitor. It may have a mechanism similar to Akti-1/2 where Pakti-L1 stabilizes the interaction between the kinase and PH domains, resulting in stabilization of the kinase-inactive "PH-in" form.[26] However, since Pakti-L1 is structurally bigger than Akti-1/2, the binding mode of Pakti-L1 should be largely different from that seen in Akti-1/2. Alternatively, Pakti-L1 interacts with a unique short sequence clustered in the region of 455−466 and allosterically inhibits the kinase activity (Supplementary Figure 2a and b). Unfortunately, this region is invisible in any of available X-ray structures of Akt, suggesting that this region may be largely unstructured. It is known that the downstream sequence, F470−Y475, docks on the "N-lobe" region when S474 is phosphorylated, resulting in activation of the kinase function.[42] Thus, if Pakti-L1 binds to this unique region and prevents the F470−Y475 region from docking, the kinase activity can be allosterically inhibited.

Since we do not have any data that enables us to rule out either hypothesis, we would like to leave open questions for the future investigations. Presumably, structural studies of the binary complex of the kinase domain with Pakti-L1 or the ternary complex with PH domain will be critical to reveal the exact inhibitory mechanism of Pakti-L1.

Conclusion. Here, we have reported thioether-macrocyclic peptide inhibitors with high Akt-selectivity generated by RaPID system. One of the inhibitors, Pakti-L1, was studied in depth and also showed a high isoform-selectivity against Akt2 over other isoforms. It is quite remarkable that even though the selection was performed against only Akt2, the selected peptides possessed isoform-selective properties. This suggests that the RaPID system could have a potential to yield isoform-selective inhibitors against various therapeutic targets of which isoform-selectivity is a strong requisite for the development of therapeutic agents. More extensive attempts by means of RaPID system against other therapeutic targets are currently underway in our laboratory.

METHODS

Preparation of ClAc^{L}Y and ^{D}Y Peptide Libraries. The mRNAs with the 4−12 repeated NNK sequences for the random region of amino acid sequence were prepared by *in vitro* transcription of their template cDNA amplified by PCR, respectively, using the primers P1, PNNK4−PNNK12, and P2 (Supplementary Table 2). The mRNA library was prepared by mixing the respective mRNAs with the 4−12 repeated NNK sequences with the following ratio, $(NNK)_4$:$(NNK)_5$:$(NNK)_6$:$(NNK)_7$:$(NNK)_8$:$(NNK)_9$:$(NNK)_{10}$:$(NNK)_{11}$:$(NNK)_{12}$ = 20^{-3}:20^{-2}:20^{-1}:1:10:10:10:10:10, adjusted to 10 μM total concentration of mRNA and denoted as a mRNA library. Two samples of 1 μM mRNA library were ligated with 1.5 μM of DNA-PEG-CCPu (Supplementary Table 2) by T4 RNA ligase at a scale of 200 μL total volume and incubated at RT for 30 min. The ligated libraries were purified by phenol-chloroform treatment and ethanol precipitation. The mRNA libraries fused with DNA-PEG-CCPu were translated in the Met-deficient FIT system at a scale of 150 μL total volume containing 50 μM ClAc^{L}Y-tRNA$^{fMet}_{CAU}$ or ClAc^{D}Y-tRNA$^{fMet}_{CAU}$,[36,37] prepared as described in Supporting Information, for 30 min at 37 °C and an additional 12 min at RT to enhance the mRNA-peptide conjugation efficiency. To quench the reaction, the samples were mixed with 15 μL of 200 mM EDTA (pH 7.5) and incubated at 37 °C for 30 min. For desalting, the samples were gel-filtered through 700 μL of fresh cross-linked dextran polymer beads, Sephadex G-25 Fine (GE Healthcare), equilibrated with PBST (10 mM Na_2HPO_4, 1.8 mM KH_2PO_4, 137 mM NaCl, 2.7 mM KCl, and 0.05% (v/v) Tween20 adjusted to pH 7.6 with HCl) twice. Preparation of the two libraries, ClAc^{L}Y (^{L}Y) library and ClAc^{D}Y (^{D}Y) library, was completed by adding an equivalent volume of 2× blocking buffer (1 M NaCl and 0.2% (w/v) acetyl-BSA in PBST) into the filtrates.

Selection Procedure by RaPID System. The following enrichment process was independently performed with the respective ^{L}Y and ^{D}Y libraries. At the first round, the ^{L}Y and ^{D}Y libraries were applied to

no protein-immobilized Ni^{2+}-NTA magnetic beads (Life Technologies, Cat. No. 10104D) twice to remove all the components tagged with the hexahistidine in the Met-deficient FIT system and undesired background beads binders from the libraries (this process is referred to as preclear below), then applied to $(His)_6$-Akt2-immobilized Ni^{2+}-NTA magnetic beads, and incubated at 4 °C for 30 min (this process is referred to as positive selection). After the incubation, the beads were washed with 500 μL of PBST four times. The washed beads were resuspended in 40 μL of reverse-transcription reaction mixture. The mRNAs remaining on the Akt2-immobilized beads were reverse-transcribed by MMLV reverse-transcriptase (Promega, Cat. No. M1705) at 42 °C for 1 h using the primer P2. The resultant cDNAs on the beads were eluted by being mixed with 200 μL of 1× PCR reaction buffer and heated at 95 °C for 5 min, with immediate separation of the supernatant from the beads. The amounts of the eluted cDNAs from the beads in the respective libraries were measured by qPCR, and the eluted cDNAs were amplified by PCR using the primer P1 and P2 for the preparation of the mRNA libraries for the next round. The aforementioned processes of (selected) library preparation, preclear, and positive selection constitute one cycle of the enrichment process.

From the second round, in the enrichment process, the reverse-transcription of mRNA to prepare the cDNAs was performed prior to the selection and the selection was performed by autodispenser machine (Nikkyo Technos Co., Ltd.). At the second round, the individual peptide libraries were prepared by *in vitro* transcription of the amplified cDNAs, ligation of the mRNA libraries with DNA-PEG-CCPu, *in vitro* translation, and reverse transcription. The libraries prepared in 5 μL of the translation scale and diluted to 100 μL with blocking buffer and PBST, the fresh magnetic beads, the wash buffer (PBST), inactive Akt2 protein, and H_2O were set in the appropriate wells of the 96-well plate. The machine was programmed to run the following processes, immobilization of Akt2 protein to Ni^{2+}-NTA magnetic beads, washing the extra Akt2 protein from the beads, and applying the respective library to the preclear and selection processes. After iterative preclear processes up to 6−12 times depending upon the rounds, the respective libraries were applied to the Akt2-immobilized beads for the selection and incubated at about 10 °C for 15−30 min. The beads were washed with 100 μL of PBST three times and resuspended with 40 μL of H_2O, and then the machine program was executed to completion. The beads were mixed with 50 μL of 2× PCR buffer and adjusted to 100 μL total volume with H_2O. The eluted cDNAs were recovered by heating the sample at 95 °C for 5 min and separating the supernatant from the beads. The recovered cDNAs were amplified by PCR and then transcribed to prepare mRNA libraries for the next round. The enrichment process was completed at the sixth round, where appreciable enrichment of the recovery rate was observed.

■ ASSOCIATED CONTENT

Ⓢ Supporting Information

This material is available free of charge *via* the Internet at http://pubs.acs.org.

■ AUTHOR INFORMATION

Corresponding Author

*E-mail: hsuga@chem.s.u-tokyo.ac.jp.

■ ACKNOWLEDGMENTS

We thank Y. Aoki for early contribution to this work, M. Hayashi for assistance with the structural analysis of Akt, and C. J. Hipolito for proofreading. We also thank M. Noguchi and F. Suizu (Hokkaido University) for the gift of PH domain in our earlier work, and H. Murakami, Y. Gotoh, and M. Higuchi (The University of Tokyo) for thoughtful discussions. This work was supported by a JSPS Grant-in-Aid for the Specially Promoted Research (21000005), a research and development projects of the Industrial Science and Technology Program in the New Energy and Industrial Technology Development Organization (NEDO) to H.S. and Grants-in-Aid for JSPS fellows to J.M. in part (21-9079).

■ REFERENCES

(1) Bellacosa, A., Kumar, C. C., Di Cristofano, A., and Testa, J. R. (2005) Activation of AKT kinases in cancer: implications for therapeutic targeting. *Adv. Cancer Res. 94*, 29−86.

(2) Romashkova, J. A., and Makarov, S. S. (1999) NF-kappaB is a target of AKT in anti-apoptotic PDGF signalling. *Nature 401*, 86−90.

(3) Staal, S. P. (1987) Molecular cloning of the akt oncogene and its human homologues AKT1 and AKT2: amplification of AKT1 in a primary human gastric adenocarcinoma. *Proc. Natl. Acad. Sci. U.S.A. 84*, 5034−5037.

(4) Sun, M., Wang, G., Paciga, J. E., Feldman, R. I., Yuan, Z. Q., Ma, X. L., Shelley, S. A., Jove, R., Tsichlis, P. N., Nicosia, S. V., and Cheng, J. Q. (2001) AKT1/PKBalpha kinase is frequently elevated in human cancers and its constitutive activation is required for oncogenic transformation in NIH3T3 cells. *Am. J. Pathol. 159*, 431−437.

(5) Bellacosa, A., de Feo, D., Godwin, A. K., Bell, D. W., Cheng, J. Q., Altomare, D. A., Wan, M., Dubeau, L., Scambia, G., Masciullo, V., Ferrandina, G., Benedetti Panici, P., Mancuso, S., Neri, G., and Testa, J. R. (1995) Molecular alterations of the AKT2 oncogene in ovarian and breast carcinomas. *Int. J. Cancer 64*, 280−285.

(6) Cheng, J. Q., Godwin, A. K., Bellacosa, A., Taguchi, T., Franke, T. F., Hamilton, T. C., Tsichlis, P. N., and Testa, J. R. (1992) AKT2, a putative oncogene encoding a member of a subfamily of protein-serine/threonine kinases, is amplified in human ovarian carcinomas. *Proc. Natl. Acad. Sci. U.S.A. 89*, 9267−9271.

(7) Yuan, Z. Q., Sun, M., Feldman, R. I., Wang, G., Ma, X., Jiang, C., Coppola, D., Nicosia, S. V., and Cheng, J. Q. (2000) Frequent activation of AKT2 and induction of apoptosis by inhibition of phosphoinositide-3-OH kinase/Akt pathway in human ovarian cancer. *Oncogene 19*, 2324−2330.

(8) Cho, H., Mu, J., Kim, J. K., Thorvaldsen, J. L., Chu, Q., Crenshaw, E. B. 3rd, Kaestner, K. H., Bartolomei, M. S., Shulman, G. I., and Birnbaum, M. J. (2001) Insulin resistance and a diabetes mellitus-like syndrome in mice lacking the protein kinase Akt2 (PKB beta). *Science 292*, 1728−1731.

(9) Brodbeck, D., Cron, P., and Hemmings, B. A. (1999) A human protein kinase Bgamma with regulatory phosphorylation sites in the activation loop and in the C-terminal hydrophobic domain. *J. Biol. Chem. 274*, 9133−9136.

(10) Tschopp, O., Yang, Z. Z., Brodbeck, D., Dummler, B. A., Hemmings-Mieszczak, M., Watanabe, T., Michaelis, T., Frahm, J., and Hemmings, B. A. (2005) Essential role of protein kinase B gamma (PKB gamma/Akt3) in postnatal brain development but not in glucose homeostasis. *Development 132*, 2943−2954.

(11) Luo, Y., Shoemaker, A. R., Liu, X., Woods, K. W., Thomas, S. A., de Jong, R., Han, E. K., Li, T., Stoll, V. S., Powlas, J. A., Oleksijew, A., Mitten, M. J., Shi, Y., Guan, R., McGonigal, T. P., Klinghofer, V., Johnson, E. F., Leverson, J. D., Bouska, J. J., Mamo, M., Smith, R. A., Gramling-Evans, E. E., Zinker, B. A., Mika, A. K., Nguyen, P. T., Oltersdorf, T., Rosenberg, S. H., Li, Q., and Giranda, V. L. (2005) Potent and selective inhibitors of Akt kinases slow the progress of tumors in vivo. *Mol. Cancer Ther. 4*, 977−986.

(12) Okuzumi, T., Fiedler, D., Zhang, C., Gray, D. C., Aizenstein, B., Hoffman, R., and Shokat, K. M. (2009) Inhibitor hijacking of Akt activation. *Nat. Chem. Biol. 5*, 484−493.

(13) Heerding, D. A., Rhodes, N., Leber, J. D., Clark, T. J., Keenan, R. M., Lafrance, L. V., Li, M., Safonov, I. G., Takata, D. T., Venslavsky, J. W., Yamashita, D. S., Choudhry, A. E., Copeland, R. A., Lai, Z., Schaber, M. D., Tummino, P. J., Strum, S. L., Wood, E. R., Duckett, D. R., Eberwein, D., Knick, V. B., Lansing, T. J., McConnell, R. T., Zhang, S., Minthorn, E. A., Concha, N. O., Warren, G. L., and Kumar, R. (2008) Identification of 4-(2-(4-amino-1,2,5-oxadiazol-3-yl)-1-ethyl-7-{[(3*S*)-3-piperidinylmethyl]oxy}-1*H*-imidazo[4,5-c]pyridin-4-yl)-2-

methyl-3-butyn-2-ol (GSK690693), a novel inhibitor of AKT kinase. *J. Med. Chem. 51*, 5663−5679.
(14) Yap, T. A., Walton, M. I., Hunter, L. J., Valenti, M., de Haven Brandon, A., Eve, P. D., Ruddle, R., Heaton, S. P., Henley, A., Pickard, L., Vijayaraghavan, G., Caldwell, J. J., Thompson, N. T., Aherne, W., Raynaud, F. I., Eccles, S. A., Workman, P., Collins, I., and Garrett, M. D. (2011) Preclinical pharmacology, antitumor activity, and development of pharmacodynamic markers for the novel, potent AKT inhibitor CCT128930. *Mol. Cancer Ther. 10*, 360−371.
(15) Grimshaw, K. M., Hunter, L. J., Yap, T. A., Heaton, S. P., Walton, M. I., Woodhead, S. J., Fazal, L., Reule, M., Davies, T. G., Seavers, L. C., Lock, V., Lyons, J. F., Thompson, N. T., Workman, P., and Garrett, M. D. (2010) AT7867 is a potent and oral inhibitor of AKT and p70 S6 kinase that induces pharmacodynamic changes and inhibits human tumor xenograft growth. *Mol. Cancer Ther. 9*, 1100−1110.
(16) Kondapaka, S. B., Singh, S. S., Dasmahapatra, G. P., Sausville, E. A., and Roy, K. K. (2003) Perifosine, a novel alkylphospholipid, inhibits protein kinase B activation. *Mol. Cancer Ther. 2*, 1093−1103.
(17) Hiromura, M., Okada, F., Obata, T., Auguin, D., Shibata, T., Roumestand, C., and Noguchi, M. (2004) Inhibition of Akt kinase activity by a peptide spanning the betaA strand of the proto-oncogene TCL1. *J. Biol. Chem. 279*, 53407−53418.
(18) Kim, D., Sun, M., He, L., Zhou, Q. H., Chen, J., Sun, X. M., Bepler, G., Sebti, S. M., and Cheng, J. Q. (2010) A small molecule inhibits Akt through direct binding to Akt and preventing Akt membrane translocation. *J. Biol. Chem. 285*, 8383−8394.
(19) Yang, L., Dan, H. C., Sun, M., Liu, Q., Sun, X. M., Feldman, R. I., Hamilton, A. D., Polokoff, M., Nicosia, S. V., Herlyn, M., Sebti, S. M., and Cheng, J. Q. (2004) Akt/protein kinase B signaling inhibitor-2, a selective small molecule inhibitor of Akt signaling with antitumor activity in cancer cells overexpressing Akt. *Cancer Res. 64*, 4394−4399.
(20) Berndt, N., Yang, H., Trinczek, B., Betzi, S., Zhang, Z., Wu, B., Lawrence, N. J., Pellecchia, M., Schonbrunn, E., Cheng, J. Q., and Sebti, S. M. (2010) The Akt activation inhibitor TCN-P inhibits Akt phosphorylation by binding to the PH domain of Akt and blocking its recruitment to the plasma membrane. *Cell Death Differ. 17*, 1795−1804.
(21) Miao, B., Skidan, I., Yang, J., Lugovskoy, A., Reibarkh, M., Long, K., Brazell, T., Durugkar, K. A., Maki, J., Ramana, C. V., Schaffhausen, B., Wagner, G., Torchilin, V., Yuan, J., and Degterev, A. (2010) Small molecule inhibition of phosphatidylinositol-3,4,5-triphosphate (PIP3) binding to pleckstrin homology domains. *Proc. Natl. Acad. Sci. U.S.A. 107*, 20126−20131.
(22) Yan, L. (2009) MK-2206: A potent oral allosteric AKT inhibitor, *AACR Meeting Abstracts 2009*, Abstract DDT01-1.
(23) Liu, R., Liu, D., Trink, E., Bojdani, E., Ning, G., and Xing, M. (2011) The Akt-specific inhibitor MK2206 selectively inhibits thyroid cancer cells harboring mutations that can activate the PI3K/Akt pathway. *J. Clin. Endocrinol. Metab. 96*, E577−585.
(24) Lindsley, C. W., Zhao, Z., Leister, W. H., Robinson, R. G., Barnett, S. F., Defeo-Jones, D., Jones, R. E., Hartman, G. D., Huff, J. R., Huber, H. E., and Duggan, M. E. (2005) Allosteric Akt (PKB) inhibitors: discovery and SAR of isozyme selective inhibitors. *Bioorg. Med. Chem. Lett. 15*, 761−764.
(25) Gilot, D., Giudicelli, F., Lagadic-Gossmann, D., and Fardel, O. (2010) Akti-1/2, an allosteric inhibitor of Akt 1 and 2, efficiently inhibits CaMKIalpha activity and aryl hydrocarbon receptor pathway. *Chem. Biol. Interact. 188*, 546−552.
(26) Wu, W. I., Voegtli, W. C., Sturgis, H. L., Dizon, F. P., Vigers, G. P., and Brandhuber, B. J. (2010) Crystal structure of human AKT1 with an allosteric inhibitor reveals a new mode of kinase inhibition. *PLoS One 5*, e12913.
(27) Litman, P., Ohne, O., Ben-Yaakov, S., Shemesh-Darvish, L., Yechezkel, T., Salitra, Y., Rubnov, S., Cohen, I., Senderowitz, H., Kidron, D., Livnah, O., Levitzki, A., and Livnah, N. (2007) A novel substrate mimetic inhibitor of PKB/Akt inhibits prostate cancer tumor growth in mice by blocking the PKB pathway. *Biochemistry 46*, 4716−4724.
(28) Obata, T., Yaffe, M. B., Leparc, G. G., Piro, E. T., Maegawa, H., Kashiwagi, A., Kikkawa, R., and Cantley, L. C. (2000) Peptide and protein library screening defines optimal substrate motifs for AKT/PKB. *J. Biol. Chem. 275*, 36108−36115.
(29) Luo, Y., Smith, R. A., Guan, R., Liu, X., Klinghofer, V., Shen, J., Hutchins, C., Richardson, P., Holzman, T., Rosenberg, S. H., and Giranda, V. L. (2004) Pseudosubstrate peptides inhibit Akt and induce cell growth inhibition. *Biochemistry 43*, 1254−1263.
(30) Shin, I., Edl, J., Biswas, S., Lin, P. C., Mernaugh, R., and Arteaga, C. L. (2005) Proapoptotic activity of cell-permeable anti-Akt single-chain antibodies. *Cancer Res. 65*, 2815−2824.
(31) Levy, D. S., Kahana, J. A., and Kumar, R. (2009) AKT inhibitor, GSK690693, induces growth inhibition and apoptosis in acute lymphoblastic leukemia cell lines. *Blood 113*, 1723−1729.
(32) Murakami, H., Ohta, A., Ashigai, H., and Suga, H. (2006) A highly flexible tRNA acylation method for non-natural polypeptide synthesis. *Nat. Methods 3*, 357−359.
(33) Ohta, A., Murakami, H., Higashimura, E., and Suga, H. (2007) Synthesis of polyester by means of genetic code reprogramming. *Chem. Biol. 14*, 1315−1322.
(34) Kawakami, T., Murakami, H., and Suga, H. (2008) Messenger RNA-programmed incorporation of multiple N-methyl-amino acids into linear and cyclic peptides. *Chem. Biol. 15*, 32−42.
(35) Kawakami, T., Murakami, H., and Suga, H. (2008) Ribosomal synthesis of polypeptoids and peptoid-peptide hybrids. *J. Am. Chem. Soc. 130*, 16861−16863.
(36) Goto, Y., Ohta, A., Sako, Y., Yamagishi, Y., Murakami, H., and Suga, H. (2008) Reprogramming the translation initiation for the synthesis of physiologically stable cyclic peptides. *ACS Chem. Biol. 3*, 120−129.
(37) Goto, Y., Katoh, T., and Suga, H. (2011) Flexizymes for genetic code reprogramming. *Nat. Protoc. 6*, 779−790.
(38) Nemoto, N., Miyamoto-Sato, E., Husimi, Y., and Yanagawa, H. (1997) In vitro virus: bonding of mRNA bearing puromycin at the 3′-terminal end to the C-terminal end of its encoded protein on the ribosome in vitro. *FEBS Lett. 414*, 405−408.
(39) Roberts, R. W., and Szostak, J. W. (1997) RNA-peptide fusions for the in vitro selection of peptides and proteins. *Proc. Natl. Acad. Sci. U.S.A. 94*, 12297−12302.
(40) Hastie, C. J., McLauchlan, H. J., and Cohen, P. (2006) Assay of protein kinases using radiolabeled ATP: a protocol. *Nat. Protoc. 1*, 968−971.
(41) Cross, D. A., Alessi, D. R., Cohen, P., Andjelkovich, M., and Hemmings, B. A. (1995) Inhibition of glycogen synthase kinase-3 by insulin mediated by protein kinase B. *Nature 378*, 785−789.
(42) Yang, J., Cron, P., Good, V. M., Thompson, V., Hemmings, B. A., and Barford, D. (2002) Crystal structure of an activated Akt/protein kinase B ternary complex with GSK3-peptide and AMP-PNP. *Nat. Struct. Biol. 9*, 940−944.

Available online at www.sciencedirect.com

SciVerse ScienceDirect

Current Opinion in Chemical Biology

Ribosomal production and *in vitro* selection of natural product-like peptidomimetics: The FIT and RaPID systems

Christopher J Hipolito and Hiroaki Suga

Bioactive natural product peptides have diverse architectures such as non-standard sidechains and a macrocyclic backbone bearing modifications. *In vitro* translation of peptides bearing these features would provide the research community with a diverse collection of natural product peptide-like molecules with a potential for drug development. The ordinary *in vitro* translation system, however, is not amenable to the incorporation of non-proteinogenic amino acids or genetic encoding of macrocyclic backbones. To circumvent this problem, flexible tRNA-acylation ribozymes (flexizymes) were combined with a custom-made reconstituted translation system to produce the flexible *in vitro* translation (FIT) system. The FIT system was integrated with mRNA display to devise an *in vitro* selection technique, referred to as the random non-standard peptide integrated discovery (RaPID) system. It has recently yielded an *N*-methylated macrocyclic peptide having high affinity (K_d = 0.60 nM) for its target protein, E6AP.

Address
Department of Chemistry, Graduate School of Science, The University of Tokyo, Tokyo 113-0033, Japan

Corresponding author: Suga, Hiroaki (hsuga@chem.s.u-tokyo.ac.jp)

Current Opinion in Chemical Biology 2012, **16**:196–203

This review comes from a themed issue on
Biocatalysis and Biotransformation
Edited by Jon S Thorson and Ben Shen

Available online 6th March 2012

1367-5931/$ – see front matter

DOI 10.1016/j.cbpa.2012.02.014

Introduction

Bioactive natural product peptides are biosynthesized by either ribosomal translation machinery or nonribosomal peptide synthetases (NRPSs) and derivatized by post-translational modification enzymes or tailoring NRPS enzymes, respectively [1]. Unlike ordinary peptides, these 'non-standard' peptides are chemically diversified with D-amino acids, unique sidechains, *N*-methylation, and macrocyclic backbones (Figure 1). In the case of NRPSs, this diversity is largely attributed to the multidomain NRPSs' ability to activate and modify amino acids before condensation. Domains are grouped into modules, and each module is in general responsible for the activation, modification and condensation of a single amino acid. Nature arranges these modules into an assembly line so that an exact peptide sequence can be produced in an NRPS-templated manner. The idea of producing custom non-standard peptides or their *de novo* libraries has attracted many researchers and driven efforts toward engineering NRPSs, but manipulating the modular NRPS components to create tailored non-standard peptides has thus far met limited success owing to their mechanistic and functional complexities. Presumably, directed evolution of NRPSs, similar to the recent work reported by Fischbach *et al.* [2] as well as Evans *et al.* [3], may lead to a solution of this herculean challenge in order to achieve the goal of constructing *de novo* libraries in the future.

Biosynthetic pathways involving post-translational modification enzymes are less complex than those involving NRPSs. In fact, genetic and mechanistic studies on such enzymes have increased our knowledge of essential recognition elements in substrates, enabling us to design non-natural substrates. Moreover, recent studies using synthetic peptides as well as coupling with *in vivo* incorporation of an artificial amino acid has allowed for the expansion of substrate repertoires [4–7]. Thus, continuing such efforts will lead us to the goal of synthesis of *de novo* libraries and, ultimately, discovering bioactive compounds with new chemical scaffolds against therapeutic targets of interest.

As a completely different technology, recent advances in artificial manipulation of the genetic code have shown the potential to produce natural product-like non-standard peptides by using translation machinery (*vide infra*). In this technology, unlike the above two biosynthetic processes, the sequences of such non-standard peptides are encoded in messenger RNA (mRNA) or its parental DNA. This feature facilitates the construction of their *de novo* libraries with high sequence complexities and, moreover, enables us to devise a one-pot screening (or selection) system to discover active non-standard peptides. In this review, we shall focus on discussing this emerging new technology.

Genetic code reprogramming as a distinct alternative approach

Genetic code reprogramming, which allows for a variety of non-standard amino acids to be incorporated by using sense codon suppressions, is a technique that was introduced within the last decade [8,9]. Genetic code reprogramming in general requires the use of a reconstituted *in vitro* translation system [10]. For instance, Forster *et al.* demonstrated in 2003 that reconstitution of only limited members of *Escherichia coli* translation factors (initiation